J. Fluid Mech. (1996), *vol.* 307, *pp.* 135–165

Evaporation and combustion of a slowly moving liquid fuel droplet: higher-order theory

By M. A. JOG[1], P. S. AYYASWAMY[2] AND I. M. COHEN[2]

[1]Department of Mechanical, Industrial, and Nuclear Engineering, University of Cincinnati, Cincinnati, OH 45221, USA

[2]Department of Mechanical Engineering and Applied Mechanics, University of Pennsylvania, Philadelphia, PA 19104, USA

(Received 21 October 1994 and in revised form 16 June 1995)

The evaporation and combustion of a single-component fuel droplet which is moving slowly in a hot oxidant atmosphere have been analysed using perturbation methods. Results for the flow field, temperature and species distributions in each phase, interfacial heat and mass transfer, and the enhancement of the mass burning rate due to the presence of convection have all been developed correct to second order in the translational Reynolds number. This represents an advance over a previous study which analysed the problem to first order in the perturbation parameter. The primary motivation for the development of detailed analytical/numerical solutions correct to second order arises from the need for such a higher-order theory in order to investigate fuel droplet ignition and extinction characteristics in the presence of convective flow. Explanations for such a need, based on order of magnitude arguments, are included in this article. With a moving droplet, the shear at the interface causes circulatory motion inside the droplet. Owing to the large evaporation velocities at the droplet surface that usually accompany drop vaporization and burning, the entire flow field is not in the Stokes regime even for low translational Reynolds numbers. In view of this, the formulation for the continuous phase is developed by imposing slow translatory motion of the droplet as a perturbation to uniform radial flow associated with vigorous evaporation at the surface. Combustion is modelled by the inclusion of a fast chemical reaction in a thin reaction zone represented by the Burke–Schumann flame front. The complete solution for the problem correct to second order is obtained by simultaneously solving a coupled formulation for the dispersed and continuous phases. A noteworthy feature of the higher-order formulation is that both the flow field and transport equations require analysis by coupled singular perturbation procedures. The higher-order theory shows that, for identical conditions, compared with the first-order theory both the flame and the front stagnation point are closer to the surface of the drop, the evaporation is more vigorous, the droplet lifetime is shorter, and the internal vortical motion is asymmetric about the drop equatorial plane. These features are significant for ignition/extinction analyses since the prediction of the location of the point of ignition/extinction will depend upon such details. This article is the first of a two-part study; in the second part, analytical expressions and results obtained here will be incorporated into a detailed investigation of fuel droplet ignition and extinction. In view of the general nature of the formulation considered here, results presented have wider applicability in the general areas of interfacial fluid mechanics and heat/material transport. They are particularly useful in microgravity

studies, in atmospheric sciences, in aerosol sciences, and in the prediction of material depletion from spherical particles.

---

1. Introduction

Rigorous analytical studies of fuel droplet evaporation, ignition, combustion and extinction in a convective flow are useful in developing models that may be used to predict and improve the performance of many combustion devices. Furthermore, studies of these phenomena at low droplet translational Reynolds numbers are of immediate application value in microgravity research (see Avedisian, Yang & Wang 1988; Jackson, Avedisian & Yang 1991; and Jackson & Avedisian 1994), in atmospheric and aerosol sciences (see Pruppacher & Klett 1980), and in studies of material depletion from spherical particles (Sadhal 1993). Although spray systems of combustion devices usually involve many drops of various sizes, it is now widely acknowledged (see, for example, Ayyaswamy 1995*a*, *b*) that the isolated drop study still merits a great deal of attention. Some background to work accomplished on droplet evaporation, ignition, combustion and extinction can be found in the review articles by Williams (1973), Sirignano & Law (1978), Law (1982), Faeth (1983), Sirignano (1983), Chigier (1983), and Ayyaswamy (1995*a*,*b*).

Sadhal & Ayyaswamy (1983) have examined the low Reynolds number translation of a drop in a gaseous medium with a strong radial field at the drop surface by using regular perturbation methods. It is noted that for liquid drops in a gaseous continuous phase, evaporation can generate a large radial velocity owing to the large density change accompanying phase change. Under these circumstances, even tiny drops (100 μm, radius) can experience inertial effects arising from the radial field, and the nonlinear inertial terms become important. Although a large uniform radial flow is an exact solution to the full Navier–Stokes equations, it cannot be superimposed on the Hadamard–Rybczynski flow even for a slowly translating drop because of the significance of the nonlinear inertial terms. On this basis, the solution for the continuous phase has been developed by considering uniform radial flow with the slow translatory motion introduced as a small perturbation. Closed-form analytical expressions for the flow fields in both phases are provided in Sadhal & Ayyaswamy (1983) by solving a coupled formulation. These flow field expressions have been employed by Gogos & Ayyaswamy (1988) and Gogos *et al.* (1986) in their investigations of the evaporation and combustion of a liquid droplet. In all of these analyses, solutions to flow and transport correct to *first order* have been obtained. In the first-order formulation, while the determination of the flow fields may be accomplished by regular perturbation procedures, the evaluation of continuous-phase heat and mass transport requires analysis by a singular perturbation method. This is due to the existence of a region of non-uniformity in the neighbourhood of the point at infinity (see Acrivos & Taylor 1962) which necessitates invoking a singular perturbation procedure where the leading-order description for the far-field temperature and mass fraction includes the perturbed velocity field. For some related discussions, see Chung, Ayyaswamy & Sadhal (1984).

It is now realized that higher-order theory and calculations for evaporation and combustion are needed for analytical/numerical investigations of droplet ignition and extinction phenomena in the presence of convective flow (Jog 1993). To appreciate this need, we first recall that the onset of droplet ignition is governed by two characteristic

time scales: the 'diffusion time' and the 'chemical reaction time'. The ratio of these time scales is the Damköhler number $\mathscr{D}$. When $\mathscr{D} \to 0$, the reaction time is very long compared to the diffusion time, and the effects due to reaction may be neglected. This is the frozen limit. When $\mathscr{D} \to \infty$, the reaction time is so short that the reaction may be assumed to take place instantaneously. This is the fast chemistry limit. Ignition and extinction phenomena are characterized by $\mathscr{D} \sim O(1)$ and represent the transition between the frozen and the fast chemistry limits. Ignition may occur when the diffusion time is of the same order of magnitude as the reaction time. The presence of convective flow introduces competition between the characteristic time scales, varying the time scales along the periphery of the droplet. Thus, the location along the droplet surface where the ignition initiates is determined in part by the effects of convection. This location is important since it determines both the nature of the flame and the extent of burning. The presence of convection also affects the ignition delay time by influencing the rates of droplet heating and vaporization. Similar considerations apply for extinction.

Ignition and extinction phenomena can be studied by allowing for finite-rate kinetics and resolving the flame structure. This may be analytically accomplished by the method of Activation Energy Asymptotics (AEA) (see, for examples, Liñán 1974; Buckmaster & Ludford 1982). AEA assumes that the chemical reaction rate has an Arrhenius temperature dependence with a large activation energy. The reaction term appearing in the non-dimensional governing equations for heat/species transport has the form $\mathscr{D} Y_O Y_F \exp(-\Theta/T)$, where Y_O and Y_F are oxidant and fuel mass fractions, respectively. Here, T is the temperature made non-dimensional by Q/c_p and Θ is the activation energy non-dimensionalized by $Q\bar{R}/c_p$. Q is the heat of combustion, $\bar{R}$ is the universal gas constant, and c_p is the specific heat at constant pressure. A distinguished limit is taken in which the activation energy Θ and the Damköhler number $\mathscr{D}$ go to infinity (Janssen 1982). The Damköhler number is taken to be of the form $\mathscr{D} = \tilde{\mathscr{D}} \exp(\Theta/T_c)$ where T_c is the non-dimensional temperature that characterizes the magnitude of $\mathscr{D}$. $\tilde{\mathscr{D}}$ is allowed to vary at most algebraically in Θ (Buckmaster & Ludford 1982), and the reaction term becomes $\tilde{\mathscr{D}} Y_O Y_F \exp[\Theta(1/T_c - 1/T)]$. When the temperature is less than T_c, the reaction term is exponentially small and the chemistry is essentially frozen. When the temperature is greater than T_c, the exponential term cannot be balanced unless the product $Y_O Y_F$ is zero. Therefore the chemistry is confined to a thin but finite reaction zone where T is close to T_c and both Y_O and Y_F are non-zero.

In order to implement AEA analysis for droplet ignition/extinction, three different regimes of interactions between fluid diffusion–convection and reaction chemistry have to be considered. These are (i) the partial burning regime in which either the oxidant or the fuel leaks through the flame to leading order, (ii) the Burke–Schumann regime in which Y_F and Y_O are zero at the flame to leading order, and (iii) the frozen chemistry regime in which the chemical reaction is negligible to leading order. Extinction may occur in the partial burning or the Burke–Schumann regime, while ignition may occur in the frozen chemistry regime. For purposes of illustration, consider the partial burning regime. In this regime, either Y_F or Y_O is non-zero to leading order at the flame. Therefore to keep the reaction term finite, temperature should be close to T_c within $O(T_c^2/\Theta)$. Let δ denote T_c^2/Θ. To predict extinction, the structure of the flame must be examined. This can be carried out by stretching the reaction zone around the location of the flame, $r = r_f(\bar{\mu})$, before extinction occurs, and solving the energy and the species conservation equations in that region. Here, r is the radial coordinate, $\bar{\mu} = \cos\theta$, and θ is the azimuthal angle. The

temperature in the reaction zone may be perturbed as $T = T_c + \delta T_r$. To solve the governing equations for energy and species in the reaction zone to $O(\delta)$, we need matching conditions for temperature and species distributions. This necessitates the development of solutions of the temperature and species conservation equations to $O(\delta)$ in the region between the drop and the flame, and in the region from the flame to the far field($r = \infty$). Typically, for a hydrocarbon fuel droplet, δ is $O(10^{-2})$. Since we are dealing with a moving drop, convective effects arising from droplet motion have to be simultaneously considered. The drop under study is translating at Reynolds number $\epsilon \sim O(10^{-1})$ with a strong radial field due to evaporation (the radial flow Reynolds number, $A_{00} \sim O(1)$). An analysis of extinction (or for that matter, ignition) will therefore have two parameters ϵ and δ, one reflecting convective flow effects and the other representing the effect of activation energy. In principle, therefore, in any perturbation study of extinction or ignition, the temperature and species variations should be expanded in terms of both ϵ and δ in both the inner and the outer regions. Such expansions would provide the required matching conditions. In its most general form, this formulation is prohibitively difficult to solve in view of the many sets of coupled equations that have to be dealt with. However, analytically and numerically consistent solutions may be obtained by considering the limit $\delta/\epsilon \ll 1$, or equivalently, for the parameters considered in fuel droplet combustion, $\delta \sim O(\epsilon^2)$. This choice satisfies two physical parametric requirements: ϵ of $O(10^{-1})$ and δ of $O(10^{-2})$. The foregoing discussion clearly establishes the need for the calculation of the temperature and the species distribution to $O(\epsilon^2)$ to provide results that can be used for the solution of the extinction problem correct to $O(\delta)$. It may also be noted that the flow field has to be determined to $O(\epsilon^2)$, as well. Similar arguments will hold for the Burke–Schumann regime and the frozen chemistry regime.

Our chief motivation for the present study has been to develop detailed mathematical analyses and solutions correct to $O(\epsilon^2)$ which can later be included in theories to predict ignition and extinction characteristics. The inclusion of higher-order perturbations greatly increases the mathematical complexities. In particular, the determination of the flow field itself becomes a singular perturbation problem because, in obtaining the second-order solution for the flow field, inertial and viscous effects become comparable far away from the droplet. As a consequence, a regular perturbation scheme is no longer adequate to obtain uniformly valid solutions even for flow fields. The degree of difficulty introduced by this complicating feature is considerable. We have solved for the fluid flow inside and outside the liquid drop and the temperature and species distribution up to and including terms of $O(\epsilon^2)$. In this treatment, while the flow fields in both phases and the transport in the gaseous phase are considered quasi-steady, the heat transport in the drop interior is treated as a transient process. This is because in the time scale of droplet heating all other processes may be regarded as quasi-steady (see Law & Sirignano 1977; Prakash & Sirignano 1980; Sundararajan & Ayyaswamy 1984). Evaporation is addressed first, and subsequently combustion is examined. Evaporation results will assist ignition studies while combustion results are useful for exploring extinction. Results obtained here compare very well with the numerical predictions of Aggarwal, Tong & Sirignano (1984).

It may be noted that even with the formal solutions presented here, to carry out detailed ignition and extinction analyses of a moving liquid hydrocarbon droplet requires additional significant effort. A great deal of activation energy theory still has to be systematically set up (see, for examples, Buckmaster & Ludford 1983; Buckmaster 1985) incorporating the present results, and then the new formulation has to be solved. These undertakings will form part of a later study.

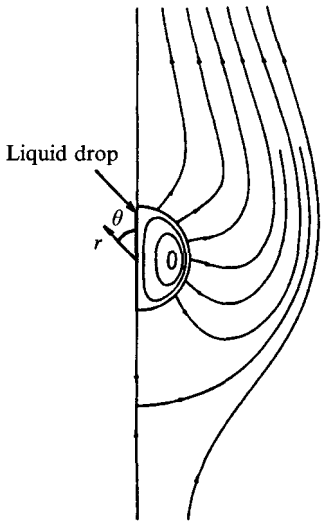

FIGURE 1. Problem schematic and coordinate system.

2. Problem formulation: evaporating droplet

Consider a single-component liquid droplet of initial radius R_0 translating with velocity $U_{\infty,0}$ in an infinite expanse of a hot, insoluble gaseous oxidant. The flow field is considered to be axisymmetric. A spherical coordinate system is used to describe the problem and the origin of the coordinate system is at the centre of the drop as shown in figure 1. The drop is initially cold at a temperature T_0. The ambient temperature T_∞ and the oxidant mass fraction $Y_{O,\infty}$ are taken to be prescribed. We note that the droplet may experience non-uniform evaporation at the surface. However, any deviation from the spherical shape caused by the non-uniform surface evaporation will be instantaneously restored by the large surface tension. Small deviations from sphericity can take place due to other effects which are quantified by Weber, Eötvös, and capillary numbers. In this paper, the Weber number($\rho_\ell U_\infty^2 R/\sigma$), the Eötvös number ($g(\rho_\ell - \rho_g)\, R^2/\sigma$), and the capillary number ($\mu_\ell U_\infty/\sigma$) are taken to be very small, and as a result the droplet will remain spherical (Sadhal & Johnson 1986). Here σ is the surface tension, μ_ℓ is the liquid-phase viscosity, and ρ_g and ρ_ℓ are the gas-phase and the liquid-phase densities, respectively. Furthermore, as shown in Sadhal & Ayyaswamy (1983), the rate of change of drop radius in a vaporizing situation is of order $\dot{R} = A_0 \rho_g/\rho_\ell$. The time scale governing substantial change in the drop size is therefore

$$t_{\dot{R}} = \frac{R}{\dot{R}} = \frac{\rho_\ell}{\rho_g}\frac{R}{A_0}.$$

The time scale for diffusion is

$$t_v = \frac{R^2}{v_g}.$$

In order that we may neglect the transient effects due to size changes on the overall process, $t_v \ll t_{\dot{R}}$, or

$$A_{00} = \frac{A_0 R}{v_g} \ll \frac{\rho_\ell}{\rho_g}.$$

For liquid–gas systems such as the one being studied here, the density ratio $\rho_\ell/\rho_g \sim 10^3$. Therefore the transient effects due to size changes may also be neglected.

Natural convection and thermodiffusion effects are considered to be negligible. In view of the small ratio of gas- to liquid-phase densities, gas-phase processes and the motion inside the drop are assumed to be quasi-steady (Sundararajan & Ayyaswamy 1984). A single effective diffusion coefficient is used for all pairs of species. To accommodate the property variations, the so called 1/3 rule is employed. It is shown in Hubbard, Denny & Mills (1975) and is recommended by Abramzon & Sirignano (1989) that the most appropriate reference temperature for property evaluations is $T_{ref} = T_s + (T_\infty - T_s)/3$, for evaporating droplets, where T_s is the temperature at the droplet surface and T_∞ is the ambient temperature. With these simplifications the governing equations for this system are

$$\nabla \cdot \boldsymbol{u}_g = 0, \tag{2.1}$$

$$\nabla \cdot \boldsymbol{u}_\ell = 0, \tag{2.2}$$

$$\rho_g \boldsymbol{u}_g \cdot \nabla \boldsymbol{u}_g + \nabla p_g = \mu_g \nabla^2 \boldsymbol{u}_g, \tag{2.3}$$

$$\rho_\ell \boldsymbol{u}_\ell \cdot \nabla \boldsymbol{u}_\ell + \nabla p_\ell = \mu_\ell \nabla^2 \boldsymbol{u}_\ell, \tag{2.4}$$

$$\frac{\partial T_\ell}{\partial t} + \boldsymbol{u}_\ell \cdot \nabla T_\ell = \alpha_\ell \nabla^2 T_\ell, \tag{2.5}$$

$$\rho_g c_{pg} \boldsymbol{u}_g \cdot \nabla T_g - k_g \nabla^2 T_g = 0, \tag{2.6}$$

$$\rho_g \boldsymbol{u}_g \cdot \nabla Y_F - \rho_g D_g \nabla^2 Y_F = 0. \tag{2.7}$$

The boundary conditions are
uniform stream at infinity:

$$u_{g,r} = U_\infty \cos\theta\,, \quad u_{g,\theta} = U_\infty \sin\theta\,, \tag{2.8}$$

$$T_g = T_\infty\,, \quad Y_F = 0. \tag{2.9}$$

finite velocity at the centre of the droplet:

$$\boldsymbol{u}_\ell|_{r=0} < \infty\,. \tag{2.10}$$

The interface conditions at $r = R$ are
continuity of tangential velocity:

$$u_{g,\theta} = u_{\ell,\theta} = u_\theta; \tag{2.11}$$

continuity of mass flux:

$$\rho_g \left(u_{g,r} - \dot{R}\right) = \rho_\ell \left(u_{\ell,r} - \dot{R}\right). \tag{2.12}$$

The normal velocity at the droplet surface can be written as

$$u_{g,r}|_{r=R} = A_0 + a(\theta), \tag{2.13}$$

where $a(\theta)$ is the translation-induced velocity governed by the thermodynamics at the interface.

We now develop a condition for the normal velocity in the liquid phase at the drop surface. The rate of mass depletion from the liquid drop is given by

$$\frac{\mathrm{d}m}{\mathrm{d}t} = \dot{m} = \rho_\ell\, 4\pi\, R^2 \dot{R}. \tag{2.14}$$

The mass depletion rate can also be calculated from the evaporation velocity at the drop surface:

$$\dot{m} = -\rho_g \int_0^{\pi} (u_{g,r} - \dot{R})|_{r=R}\, 2\pi R \sin\theta\, R\, \mathrm{d}\theta \tag{2.15}$$

$$= -2\pi R^2 \rho_g \int_0^{\pi} (u_{g,R} - \dot{R}) \sin\theta\, \mathrm{d}\theta. \tag{2.16}$$

The evaporation velocity at the drop surface can be substituted from equation (2.13) to give

$$\dot{m} = -4\pi R^2 \rho_g \left(A_0 - \dot{R} + \int_0^{\pi} \tfrac{1}{2} a(\theta) \sin\theta\, \mathrm{d}\theta \right). \tag{2.17}$$

From equations (2.14) and (2.17), we have

$$\dot{R}\left(1 - \frac{\rho_g}{\rho_\ell}\right) = -\frac{\rho_g}{\rho_\ell}\left(A_0 + \int_0^{\pi} \tfrac{1}{2} a(\theta) \sin\theta\, \mathrm{d}\theta \right). \tag{2.18}$$

Equation (2.12) can be rearranged as

$$u_{\ell,R} = \dot{R}\left(1 - \frac{\rho_g}{\rho_\ell}\right) + \frac{\rho_g}{\rho_\ell} u_{g,R}. \tag{2.19}$$

Combining equations (2.18) and (2.19) and simplifying we get

$$u_\ell|_{r=R} = \frac{\rho_g}{\rho_\ell}\left\{ a(\theta) - \frac{1}{2}\int_0^{\pi} a(\theta) \sin\theta\, \mathrm{d}\theta \right\}. \tag{2.20}$$

For a typical liquid hydrocarbon droplet such as the one being considered in this study, ρ_g/ρ_ℓ is $O(10^{-3})$. The quantity $a(\theta)$ is the normal component of the translation-induced gas velocity which is expected to be of the same order as the translation ($O(\epsilon)$) or smaller. Therefore, the magnitude of the radial component of the liquid velocity at the droplet surface, $u_\ell|_{r=R}$, will be orders of magnitude smaller than the normal velocity in the continuous phase and therefore taken to be essentially zero. This approximation allows us to obtain closed-form analytical solutions for the flow field without much loss of accuracy. Thus,

$$u_\ell|_{r=R} \doteq 0. \tag{2.21}$$

Further boundary conditions are
continuity of shear stress:

$$\mu_g \left[r \frac{\partial}{\partial r}\left(\frac{u_{g,\theta}}{r}\right) + \frac{1}{r}\frac{\partial u_{g,r}}{\partial \theta} \right]_{r=R} = \mu_\ell \left[r \frac{\partial}{\partial r}\left(\frac{u_{\ell,\theta}}{r}\right) + \frac{1}{r}\frac{\partial u_{\ell,r}}{\partial \theta} \right]_{r=R}; \tag{2.22}$$

normal stress balance:

$$p_g + \frac{2\sigma}{R} - \tfrac{4}{3}\mu_g \left[\frac{\partial u_{g,r}}{\partial r} - \frac{u_{g,r}}{r} - \frac{1}{2r\sin\theta}\frac{\partial}{\partial \theta}\left(u_{g,\theta}\sin\theta\right) \right]$$

$$= p_\ell - \tfrac{4}{3}\mu_\ell \left[\frac{\partial u_{\ell,r}}{\partial r} - \frac{u_{\ell,r}}{r} - \frac{1}{2r\sin\theta}\frac{\partial}{\partial \theta}\left(u_{\ell,\theta}\sin\theta\right) \right]. \tag{2.23}$$

The equation for the normal stress balance has been written here for completeness but need not be considered any further in view of the large surface tension and the assumed spherical shape of the drop.

The final boundary conditions are
temperature continuity:

$$T_g|_{r=R} = T_\ell|_{r=R}\,; \tag{2.24}$$

the impermeability condition:

$$D_g \frac{\partial Y_F}{\partial r} = -(1 - Y_F)u_{gr}; \tag{2.25}$$

interfacial heat balance:

$$k_g \frac{\partial T_g}{\partial r} - \rho_g \left(u_g - \dot{R}\right) L = k_\ell \frac{\partial T_\ell}{\partial r}. \tag{2.26}$$

Y_F at the droplet surface is calculated using the Clausius–Clapeyron equation.
In the above, u is the velocity, T denotes the temperature, p is the pressure, Y_F denotes the fuel mass fraction, α is the thermal diffusivity, ρ is the density, k is thermal conductivity, μ is the viscosity, D_g is the mass diffusivity, σ is the surface tension, t is the time, R is the drop radius, and the subscripts g and ℓ are used to denote the gas phase and the liquid phase, respectively.

3. Solution for the flow field: gaseous phase

In order to non-dimensionalize the governing equations it is appropriate to scale $\boldsymbol{u}_{g,0}$ with A_0, and $\boldsymbol{u}'_g$ and $\boldsymbol{u}'_\ell$ with U_∞. Thus $\boldsymbol{u}^*_{g,0} = \boldsymbol{u}_{g,0}/A_0$, $\boldsymbol{u}'^*_g = \boldsymbol{u}'_g/U_\infty$, $\boldsymbol{u}'^*_\ell = \boldsymbol{u}'_\ell/U_\infty$, $r^* = r/R$, $\epsilon = U_\infty R/\nu$, $A_{00} = A_0 R/\nu$, $p^*_{g,0} = p_{g,0}/(A_0\mu_g/R)$, $p'^*_g = p'_g/(U_\infty\mu_g/R)$, $p'^*_\ell = p'_\ell/(U_\infty\mu_\ell/R)$ and $\nabla^* = R\nabla$. We define a non-dimensional velocity in the gas phase as $\boldsymbol{u}^*_g = \boldsymbol{u}_g R/\nu_g$, and in the liquid phase as $\boldsymbol{u}^*_\ell = \boldsymbol{u}_\ell R/\nu_g$. A perturbation scheme can now be introduced as $\boldsymbol{u}' = \boldsymbol{u}_1 + \epsilon\boldsymbol{u}_2 + \cdots$, $p' = p_1 + \epsilon p_2 + \cdots$, where u' and p' are dimensionless variables with the asterisks dropped. Hence we have

$$\boldsymbol{u}_g = A_{00}\boldsymbol{u}_{g,0} + \epsilon\boldsymbol{u}_{g,1} + \epsilon^2\boldsymbol{u}_{g,2} + \cdots, \tag{3.1}$$

$$p_g = A_{00}p_{g,0} + \epsilon p_{g,1} + \epsilon^2 p_{g,2} + \cdots, \tag{3.2}$$

$$\boldsymbol{u}_\ell = \epsilon\boldsymbol{u}_{\ell,1} + \epsilon^2\boldsymbol{u}_{\ell,2} + \cdots, \tag{3.3}$$

$$p_\ell = A_{00}p_{\ell,0} + \epsilon p_{\ell,1} + \epsilon^2 p_{\ell,2} + \cdots. \tag{3.4}$$

Uniform evaporation at the droplet surface does not induce flow inside the droplet and $\boldsymbol{u}_{\ell,0} = 0$. We introduce stream functions ψ_g and ψ_ℓ for the gas and liquid phases respectively. The continuity equations are identically satisfied by letting the velocities be

$$u_{g,r} = \frac{1}{r^2 \sin\theta}\frac{\partial\psi_g}{\partial\theta}, \tag{3.5}$$

$$u_{g,\theta} = -\frac{1}{r\sin\theta}\frac{\partial\psi_g}{\partial r}, \tag{3.6}$$

$$u_{\ell,r} = \frac{1}{r^2\sin\theta}\frac{\partial\psi_\ell}{\partial\theta}, \tag{3.7}$$

$$u_{\ell,\theta} = -\frac{1}{r\sin\theta}\frac{\partial\psi_\ell}{\partial r}. \tag{3.8}$$

In view of equations (3.1) and (3.3) we may write

$$\psi_g = A_{00}\psi_{g,0} + \epsilon\psi_{g,1} + \epsilon^2\psi_{g,2} + \cdots, \tag{3.9}$$

$$\psi_\ell = \epsilon\psi_{\ell,1} + \epsilon^2\psi_{\ell,2} + \cdots. \tag{3.10}$$

The normal velocity at the droplet surface is $A_0 + A_1(\theta)$, where $A_1(\theta)$ is the translation-induced velocity governed by the thermodynamics at the interface. We expand $A_1(\theta)$ in terms of an infinite series of Legendre polynomials (P_n). Hence, in non-dimensional form, the normal velocity at the interface is

$$u_{g,r}|_{r=1} = A_{00} + \epsilon \sum_{n=1}^{\infty} A_{n1} P_n(\bar{\mu}) + \epsilon^2 \sum_{n=1}^{\infty} A_{n2} P_n(\bar{\mu}) + \cdots,$$

where, $\bar{\mu} = \cos\theta$. We assume that the perturbed normal velocity at the interface has the same angular behaviour as the variable causing it, namely the translational field. Therefore,

$$u_{g,r}|_{r=1} = A_{00} + \epsilon (A_{01} + \bar{\mu} A_{11}) + \epsilon^2 \left(A_{02} + \bar{\mu} A_{12} + \tfrac{1}{2}(3\bar{\mu}^2 - 1) A_{22}\right) + \cdots.$$

3.1. *Leading-order inner solutions*

In the inner region of the gaseous-phase flow, that is where $r = O(1)$, we may write the governing equation in terms of the stream function ψ_g as

$$\frac{1}{r^2} \frac{\partial(\psi_g, \mathrm{D}_r^2 \psi_g)}{\partial(r, \bar{\mu})} + \frac{2}{r^2} \mathrm{D}_r^2 \psi_g \, \mathrm{L}_r \psi_g = \frac{1}{A_{00}} \mathrm{D}_r^4 \psi_g, \tag{3.11}$$

where

$$\mathrm{D}_r^2 = \frac{\partial^2}{\partial r^2} + \frac{1 - \bar{\mu}^2}{r^2} \frac{\partial^2}{\partial \bar{\mu}^2}, \tag{3.12}$$

$$\mathrm{L}_r = \frac{\bar{\mu}}{1 - \bar{\mu}^2} \frac{\partial}{\partial r} + \frac{1}{r} \frac{\partial}{\partial \bar{\mu}}. \tag{3.13}$$

In order to satisfy the velocity variation at the droplet interface and the uniform flow at infinity, the stream function is expanded in terms of Gegenbauer polynomials as

$$\psi_{g,m}(r, \bar{\mu}) = \sum_{n=0}^{\infty} \psi_{g,m}^n(r) C_{n+1}^{-1/2}(\bar{\mu}). \tag{3.14}$$

Only the terms required to satisfy the boundary conditions are retained in this expansion.

Using equations (3.9) and (3.11), the leading-order inner solution which satisfies the boundary condition at the droplet can be easily obtained as

$$\psi_{g,0} = -\bar{\mu}. \tag{3.15}$$

The expansion scheme (equation (3.1)) can be substituted into the momentum equation to compare the importance of inertia and viscous terms in the entire flow field. The solutions for stream functions (presented later in this paper) are used to estimate the large-r behaviour of the inertia and the viscous terms:

$$\text{inertia terms}: \quad A_{00}^2 \boldsymbol{u}_{g,0} \cdot \nabla \boldsymbol{u}_{g,0} + A_{00}\epsilon \left(\boldsymbol{u}_{g,0} \cdot \nabla \boldsymbol{u}_{g,1} + \boldsymbol{u}_{g,1} \cdot \nabla \boldsymbol{u}_{g,0}\right) + \epsilon^2 \left(A_{00} \boldsymbol{u}_{g,0} \cdot \nabla \boldsymbol{u}_{g,2} + \boldsymbol{u}_{g,1} \cdot \nabla \boldsymbol{u}_{g,1} + A_{00} \boldsymbol{u}_{g,2} \cdot \nabla \boldsymbol{u}_{g,0}\right)$$

$$\text{as } r \to \infty \qquad \sim O\left(\frac{1}{r^5}\right) : O\left(\frac{\epsilon}{r^5}\right) : O\left(\frac{\epsilon^2}{r^3}\right);$$

$$\text{viscous terms}: \quad A_{00} \nabla^2 \boldsymbol{u}_{g,0} + \epsilon \nabla^2 \boldsymbol{u}_{g,1} + \epsilon^2 \nabla^2 \boldsymbol{u}_{g,2}$$

$$\text{as } r \to \infty$$
$$\sim O\left(\frac{1}{r^4}\right) : O\left(\frac{\epsilon}{r^4}\right) : O\left(\frac{\epsilon^2}{r^3}\right).$$

In obtaining the flow field solutions for the inner region, we have neglected the terms of order (ϵ^2/r^3) while retaining the terms of order $(1/r^5)$. Clearly, this assumption will break down for $r > 1/\epsilon$. Therefore, the inner solutions are not uniformly valid in the entire flow field. Thus a regular perturbation scheme will not be adequate to obtain uniformly valid solutions. A singular perturbation approach needs to be adopted and the governing equations have to be rescaled in the outer region ($\epsilon r > 1$).

Following Proudman & Pearson (1957) we define a strained coordinate for the outer region as $\rho = \epsilon r$ and the stream function as $\Psi_g = \epsilon^2 \psi_g$. In the outer region it is inappropriate to scale velocity by the evaporation velocity A_0. By scaling velocity in the outer region by U_∞ and defining a non-dimensional velocity as $U_g^* = U_g R/v_g$ we have, with the asterisks dropped,

$$U_g = \epsilon U_{g,0} + \epsilon^2 U_{g,1} + \cdots \tag{3.16}$$

and

$$\Psi_g = \epsilon \Psi_{g,0} + \epsilon^2 \Psi_{g,1} + \cdots. \tag{3.17}$$

The governing equation for the outer region becomes

$$\frac{1}{\rho^2}\frac{\partial(\Psi_g, \mathrm{D}_\rho^2 \Psi_g)}{\partial(\rho, \bar{\mu})} + \frac{2}{\rho^2}\mathrm{D}_\rho^2 \Psi_g \, \mathrm{L}_\rho \Psi_g = \mathrm{D}_\rho^4 \Psi_g. \tag{3.18}$$

The leading-order outer solution is a uniform stream

$$\Psi_{g,0} = \tfrac{1}{2}\rho^2(1 - \bar{\mu}^2). \tag{3.19}$$

3.2. *First-order inner solution*

To order ϵ the governing equation for $\psi_{g,1}$ becomes

$$\mathrm{D}_r^4 \psi_{g,1} = \frac{A_{00}}{r^2}\left(\frac{\partial}{\partial r} - \frac{2}{r}\right)\mathrm{D}_r^2 \psi_{g,1}. \tag{3.20}$$

The solution for $\psi_{g,1}$ is

$$\psi_{g,1} = -A_{01}\bar{\mu} + \tfrac{1}{2} f(r)(1 - \bar{\mu}^2) \tag{3.21}$$

where

$$f(r) = \frac{B}{r} + C\left\{\frac{1}{r}\int_1^r \left[\left(\frac{\xi}{A_{00}}\right)^4 + \left(\frac{\xi}{A_{00}}\right)^3\right] \mathrm{e}^{-A_{00}/\xi} \mathrm{d}\xi\right\} + Er^4 + Fr^2. \tag{3.22}$$

The coefficients E and F are obtained by matching this inner solution with the outer solution. Matching with (3.19) we obtain $E = -C/(5A_{00}^4)$ and $F = 1 + C/(6A_{00}^2)$. Thus we recover the solution for $\psi_{g,1}$ given by Sadhal & Ayyaswamy (1983) as

$$\psi_{g,1} = -A_{01}\bar{\mu} + \left(r^2 + \frac{B}{r} + C\left\{\frac{1}{r}\int_1^r \left[\left(\frac{\xi}{A_{00}}\right)^4 + \left(\frac{\xi}{A_{00}}\right)^3\right] \mathrm{e}^{-A_{00}/\xi} \mathrm{d}\xi \right.\right.$$
$$\left.\left. - \frac{1}{5}\left(\frac{r}{A_{00}}\right)^4 + \frac{1}{6}\left(\frac{r}{A_{00}}\right)^2\right\}\right)(1 - \bar{\mu}^2)/2. \tag{3.23}$$

3.3. *Second-order inner solution*

Stream function $\psi_{g,2}$ satisfies the equation

$$D_r^4\psi_{g,2} - \frac{A_{00}}{r^2}\left(\frac{\partial}{\partial r} - \frac{2}{r}\right)D_r^2\psi_{g,2} = \frac{C}{2A_{00}}\frac{e^{-A_{00}/r}}{r^4}[A_{01} + \bar{\mu}f(r)](1-\bar{\mu}^2). \tag{3.24}$$

Let

$$\psi_{g,2} = -A_{02}\bar{\mu} + \psi_{g,2}^1(r)(1-\bar{\mu}^2) + \psi_{g,2}^2(r)\bar{\mu}(1-\bar{\mu}^2). \tag{3.25}$$

This gives

$$\left[\frac{d^2}{dr^2} - \frac{A_{00}}{r^2}\left(\frac{d}{dr} - \frac{2}{r}\right) - \frac{2}{r^2}\right]\left[\frac{d^2}{dr^2} - \frac{2}{r^2}\right]\psi_{g,2}^1(r) = \frac{CA_{01}}{2A_{00}}\frac{e^{-A_{00}/r}}{r^4}. \tag{3.26}$$

The solution for $\psi_{g,2}^1(r)$ can be obtained as

$$\psi_{g,2}^1(r) = \frac{C_1}{r}\int_1^r\left[\left(\frac{\xi}{A_{00}}\right)^4 + \left(\frac{\xi}{A_{00}}\right)^3\right]e^{-A_{00}/\xi}d\xi + C_2r^4 + C_3r^2 + \frac{C_4}{r} - \frac{CA_{01}}{2A_{00}^3}\frac{1}{r}\int_1^r \xi^2 e^{-A_{00}/\xi}d\xi. \tag{3.27}$$

For large r, $\psi_{g,2}^1(r)$ behaves as

$$\psi_{g,2}^1(r) \sim \left(C_2 + \frac{C_1}{5A_{00}^4}\right)r^4 + \left(C_3 - \frac{CA_{01}}{6A_{00}^3} - \frac{C_1}{6A_{00}^2}\right)r^2 + O(r). \tag{3.28}$$

Stream function $\psi_{g,2}^2(r)$ satisfies

$$\left[\frac{d^2}{dr^2} - \frac{A_{00}}{r^2}\left(\frac{d}{dr} - \frac{2}{r}\right) - \frac{6}{r^2}\right]\left[\frac{d^2}{dr^2} - \frac{6}{r^2}\right]\psi_{g,2}^2(r) = \frac{Cf(r)}{2A_{00}}\frac{e^{-A_{00}/r}}{r^4}. \tag{3.29}$$

Let $x = r/A_{00}$ and

$$\left[\frac{d^2}{dx^2} - \frac{6}{x^2}\right]\psi_{g,2}^2(x) = y(x). \tag{3.30}$$

Hence,

$$\left[\frac{d^2}{dx^2} - \frac{1}{x^2}\left(\frac{d}{dx} - \frac{2}{x}\right) - \frac{6}{x^2}\right]y(x) = \frac{Cf(x)}{2A_{00}}\frac{e^{-1/x}}{x^4}. \tag{3.31}$$

Solutions for the homogeneous part of equation (3.31) are

$$y_1 = (1 + 6x + 18x^2 + 24x^3)\,e^{-1/x}, \tag{3.32}$$

$$y_2 = 6x^2 - 24x^3. \tag{3.33}$$

To ensure proper behaviour as $x \to \infty$, the solution can also be constructed in powers of $1/x$ as (Sadhal 1993)

$$y_3 = \sum_{k=0}^{\infty}\frac{(k+3)!5!(-1)^k}{k!3!(k+5)!}x^{-(k+2)}. \tag{3.34}$$

Using the method of variation of parameters, the complete solution can be obtained as

$$y(x) = d_1y_3 - \frac{1}{12}CA_{00}e^{-1/x} - \frac{Cy_1}{2A_{00}}\int^x\frac{y_2f_1}{x^4}dx + \frac{Cy_2}{2A_{00}}\int^x\frac{y_1f_1}{x^4}dx, \tag{3.35}$$

where $f_1(x) = f(x) - A_{00}^2 x^2$. The two linearly independent solutions for equation (3.30) are x^3 and $1/x^2$. Using the method of variation of parameters the complete solution can be obtained as

$$\psi_{g,2}^2(x) = d_3 x^3 + \frac{d_4}{x^2} + \frac{x^3}{5}\int_{1/A_{00}}^{x} \frac{y(x)}{x^2}\mathrm{d}x - \frac{1}{5x^2}\int_{1/A_{00}}^{x} x^3 y(x)\mathrm{d}x. \tag{3.36}$$

It can be shown that for large x, $\psi_{g,2}^2(x)$ behaves as

$$\psi_{g,2}^2(x) \sim \left(d_3 + \frac{\Omega'}{5}\right) x^3 + \frac{CA_{00}}{48} x^2 + O(x)\,. \tag{3.37}$$

In terms of r,

$$\psi_{g,2}^2(r) \sim \left(d_3 + \frac{\Omega'}{5}\right) \frac{r^3}{A_{00}^3} + \frac{C}{48A_{00}} r^2 + O(r) \tag{3.38}$$

where $\Omega' = \int_{1/A_{00}}^{\infty} y(\xi)/\xi^2 \mathrm{d}\xi$. Therefore, for large r, the behaviour of $\epsilon\psi_{g,0} + \epsilon^2\psi_{g,1} + \epsilon^3\psi_{g,2}$ written in terms of the outer variable is

$$\begin{aligned}\epsilon\psi_{g,0} + \epsilon^2\psi_{g,1} + \epsilon^3\psi_{g,2} \sim{}& \tfrac{1}{2}(1-\bar{\mu}^2)\rho^2 - A_{00}\bar{\mu}\epsilon + \tfrac{1}{2}(1-\bar{\mu}^2)\frac{C\rho}{6}A_{00}\epsilon \\ &+ \left(C_2 + \frac{C_1}{5A_{00}^4}\right)\frac{\rho^4}{\epsilon^2}(1-\bar{\mu}^2) + \left(C_3 - \frac{CA_{01}}{6A_{00}^3} - \frac{C_1}{6A_{00}^2}\right)\rho^2(1-\bar{\mu}^2) \\ &+ \bar{\mu}(1-\bar{\mu}^2)\left(d_3 + \frac{\Omega'}{5}\right)\frac{\rho^3}{A_{00}^3} + \bar{\mu}(1-\bar{\mu}^2)\frac{C\rho^2}{48A_{00}}\epsilon + O(\epsilon^2).\end{aligned} \tag{3.39}$$

3.4. *First-order outer solution*

The governing equation for $\Psi_{g,1}$ is

$$\frac{(1-\bar{\mu}^2)}{\rho}\frac{\partial \mathrm{D}_\rho^2 \Psi_{g,1}}{\partial \bar{\mu}} + \bar{\mu}\frac{\partial \mathrm{D}_\rho^2 \Psi_{g,1}}{\partial \rho} = \mathrm{D}_\rho^4 \Psi_{g,1}. \tag{3.40}$$

The substitution $\mathrm{D}_\rho^2 \Psi_{g,1} = \exp(\rho\bar{\mu}/2)\Phi$ gives

$$\left(\mathrm{D}_\rho^2 - \tfrac{1}{4}\right)\Phi = 0 \tag{3.41}$$

and

$$\mathrm{D}_\rho^2 \Psi_{g,1} = \mathrm{e}^{\rho\bar{\mu}/2} \sum_{n=1}^{\infty} A_n (\tfrac{1}{2}\rho)^{1/2} K_{n+1/2}(\tfrac{1}{2}\rho) Q_n(\bar{\mu}). \tag{3.42}$$

Here $Q_n(\bar{\mu}) = \int_{-1}^{\bar{\mu}} P_n(\bar{\mu})\,\mathrm{d}\bar{\mu}$. The solution for $\Psi_{g,1}$, such that $\Psi_{g,0} + \epsilon\Psi_{g,1}$ matches with the inner solution (equation (3.39)), can be obtained as

$$\Psi_{g,1} = -A_{00}\bar{\mu} + \frac{C}{6A_{00}}(1+\bar{\mu})\left\{1 - \exp\left[-\tfrac{1}{2}\rho(1-\bar{\mu})\right]\right\}. \tag{3.43}$$

The matching procedure also suggests

$$C_2 = -\frac{C_1}{5A_{00}^4}, \quad C_3 = \frac{C_1}{6A_{00}^2} + \frac{CA_{01}}{6A_{00}^3} - \frac{C}{48A_{00}}, \quad d_3 = -\frac{\Omega'}{5}\,.$$

4. Solution for the flow field: liquid phase

The governing equation for ψ_ℓ can be written as

$$\frac{1}{r^2}\frac{\partial(\psi_\ell, \mathrm{D}_r^2\psi_\ell)}{\partial(r,\bar{\mu})} + \frac{2}{r^2}\mathrm{D}_r^2\psi_\ell L_r\psi_\ell = \frac{1}{\phi_v}\mathrm{D}_r^4\psi_\ell, \tag{4.1}$$

where $\phi_v = \nu_g/\nu_\ell$.

4.1. *First-order solution*

Using equation (3.10) we find that $\psi_{\ell,1}$ satisfies

$$\mathrm{D}_r^4\psi_{\ell,1} = 0. \tag{4.2}$$

In view of equations (2.11) and (2.22), we take $\psi_{\ell,1} = \ell_0(r)(1-\bar{\mu}^2)$. Therefore

$$\left(\frac{\mathrm{d}^2}{\mathrm{d}r^2} - \frac{2}{r^2}\right)^2 \ell_0(r) = 0. \tag{4.3}$$

The solution for ψ_{ℓ_1} satisfying (2.10) is

$$\psi_{\ell,1} = \hat{B}(r^4 - r^2)(1-\bar{\mu}^2). \tag{4.4}$$

4.2. *Second-order solution*

For consistency we take

$$\psi_{\ell,2} = \ell_1(r)(1-\bar{\mu}^2) + \ell_2(r)\bar{\mu}(1-\bar{\mu}^2). \tag{4.5}$$

Equation (4.1) gives

$$\left(\frac{\mathrm{d}^2}{\mathrm{d}r^2} - \frac{2}{r^2}\right)^2 \ell_1(r) = 0, \tag{4.6}$$

$$\left(\frac{\mathrm{d}^2}{\mathrm{d}r^2} - \frac{6}{r^2}\right)^2 \ell_2(r) = 0, \tag{4.7}$$

and the solution satisfying (2.10) is

$$\psi_{\ell,2} = B_1(r^4 - r^2)(1-\bar{\mu}^2) + B_2(r^5 - r^3)\bar{\mu}(1-\bar{\mu}^2). \tag{4.8}$$

The integration constants in the solutions for the flow field in the liquid phase and in the gaseous phase are obtained by satisfying the interface conditions. These integration constants are $\hat{B}$ (in equation (4.4)), B_1 and B_2 (in (4.8)), B and C (in (3.23)), C_1 and C_4 (in (3.27)), d_1 (in (3.35)) and d_4 (in (3.36)). The expressions for $\hat{B}$, B, and C can be found in Sadhal & Ayyaswamy (1983) and are not repeated here for brevity. With $\phi_\mu = \mu_g/\mu_\ell$,

$$C_1 = \frac{\left(\frac{3}{2}+\phi_\mu\right)\left[A_{12}A_{00}^4 + \frac{1}{8}CA_{00}^3 + CA_{01}A_{00}\left(\mathrm{e}^{-A_{00}} - 1\right)\right] - \frac{1}{2}CA_{01}A_{00}^2\phi_\mu}{-3 + \left(\frac{3}{2}+\phi_\mu\right)A_{00}^2 + 3\left[1 + A_{00} - \frac{1}{3}\phi_\mu A_{00}^2\right]\mathrm{e}^{-A_{00}}},$$

$$C_4 = \frac{A_{12}}{2} + C\left(\frac{1}{48A_{00}} - \frac{A_{01}}{6A_{00}^3}\right) + C_1\left(\frac{1}{5A_{00}^4} - \frac{1}{6A_{00}^2}\right),$$

$$B_1 = \frac{C_1\phi_\mu}{6A_{00}^2}(\mathrm{e}^{-A_{00}} - 1) + \frac{CA_{01}\phi_\mu}{6A_{00}^3}\left[(1 - \frac{A_{00}}{2})\mathrm{e}^{-A_{00}} - 1 - \frac{A_{00}^2}{8A_{01}}\right] + \frac{A_{12}\phi_\mu}{6},$$

$$B_2 = -\frac{A_{22}}{2} - \frac{\Omega'}{2A_{00}^3},$$

$$d_1 = \frac{A_{22}\left(2-\frac{5}{\phi_\mu}\right) - \frac{\Omega'}{A_{00}^3}\left(2+\frac{5}{\phi_\mu}\right) - y_p + \frac{C}{12A_{00}}e^{-A_{00}}}{\sum_{k=0}^{\infty}\frac{(k+3)!5!(-1)^k}{k!3!(k+5)!}A_{00}{}^k},$$

$$d_4 = \frac{A_{22}}{2A_{00}^2} + \frac{\Omega'}{5A_{00}^5}.$$

Here

$$y_p = \frac{C}{12A_{00}}\sum_{n=2}^{\infty}\frac{(-A_{00})^n}{(n-2)!(n+2)(n+3)} \times \xi_1 + \frac{C}{12A_{00}}\left(\frac{24}{A_{00}^3} - \frac{6}{A_{00}^2}\right) \times \xi_2$$

where

$$\xi_1 = -4C\ln(A_{00}) - \frac{4C}{A_{00}} + \frac{31}{20}CA_{00} + \frac{1}{30}CA_{00}^2 + (24-3A_{00})(B+\alpha_2'C) + 6C\sum_{n=3}^{\infty}(-A_{00})^n\frac{n^2+10n+20}{n(n-1)(n+4)!},$$

$$\xi_2 = -\frac{C}{6}\sum_{n=4}^{\infty}\frac{(-A_{00})^n}{(n-4)!n^2(n+1)} - \left(\frac{B+\alpha_2'C}{A_{00}} + \frac{C\ln A_{00}}{30}\right)\sum_{n=6}^{\infty}\frac{(-A_{00})^n}{(n-6)!n(n-1)(n-2)} + C\sum_{m=2}^{\infty}\sum_{n=6}^{\infty}\frac{(-A_{00})^{m+n-1}}{(m+2)!(m-1)(m+4)(m+n-1)(n-6)!(n-1)(n-2)} - \frac{C}{8}\sum_{n=5}^{\infty}\frac{(-A_{00})^n}{(n-5)!n^2(n-1)} - C\sum_{n=6}^{\infty}\frac{(-A_{00})^n(1/n-\ln A_{00})}{30(n-6)!n(n-1)(n-2)},$$

$$\alpha_2' = \frac{A_{00}}{30}\left[-\gamma - \ln(A_{00}) + Ei(-A_{00}) + \frac{61}{30}\right] - \left[\frac{1}{5A_{00}^4} + \frac{1}{5A_{00}^3} - \frac{1}{15A_{00}^2} + \frac{1}{30A_{00}} - \frac{1}{30}\right]e^{-A_{00}}$$

and $Ei(-x)$ is the exponential integral

$$Ei(-x) = -\int_x^{\infty}\frac{e^{-\xi}}{\xi}d\xi. \tag{4.9}$$

The quantity $\gamma = 0.57721\ldots$ is the Euler–Mascheroni constant.

5. Drag force calculations

The drag force on the liquid drop consists of contributions from the viscous stresses, the pressure, and the momentum flux at the interface. The leading-order terms are given by Sadhal & Ayyaswamy (1983). We calculate the terms up to and including $O(\epsilon)$. The drag force is non-dimensionalized by $\mu_g U_\infty R$.

The non-dimensional viscous drag force is given by

$$F_\mu^* = \frac{2\pi}{\epsilon}\int_0^\pi (\tau_{r\theta}\sin\theta - \tau_{rr}\cos\theta)|_{r=1}\sin\theta\,\mathrm{d}\theta, \tag{5.1}$$

where

$$\tau_{r\theta} = \mu_g\left[r\frac{\partial}{\partial r}\left(\frac{u_{g,\theta}}{r}\right) + \frac{1}{r}\frac{\partial u_{g,r}}{\partial\theta}\right] \quad \text{and} \quad \tau_{rr} = 2\mu_g\frac{\partial u_{g,r}}{\partial r}, \tag{5.2}$$

or

$$F_\mu^* = \frac{4\pi C}{3}\left[\left(\frac{2}{A_{00}^4}+\frac{2}{A_{00}^3}+\frac{1}{A_{00}^2}\right)\mathrm{e}^{-A_{00}} - \frac{2}{A_{00}^4}\right] + \epsilon\frac{4\pi}{3}\left\{2C_1\left[\left(\frac{2}{A_{00}^4}+\frac{2}{A_{00}^3}+\frac{1}{A_{00}^2}\right)\mathrm{e}^{-A_{00}} - \frac{2}{A_{00}^4}\right] - \frac{CA_{01}}{A_{00}^2}\mathrm{e}^{-A_{00}}\right\} + O(\epsilon^2). \tag{5.3}$$

The non-dimensional pressure drag is

$$\begin{aligned} F_p^* &= \frac{2\pi}{\epsilon}\int_0^\pi p_g|_{r=1}\sin 2\theta\,\mathrm{d}\theta \\ &= \frac{4\pi}{3}\left\{A_{00}A_{11} - C\left[\left(\frac{2}{A_{00}^4}+\frac{1}{A_{00}^3}\right)\mathrm{e}^{-A_{00}} - \frac{2}{A_{00}^4}+\frac{1}{A_{00}^3}\right]\right\} \\ &\quad + \epsilon\frac{4\pi}{3}\left\{A_{00}A_{12}+A_{01}A_{11} - 2C_1\left[\left(\frac{2}{A_{00}^4}+\frac{1}{A_{00}^3}\right)\mathrm{e}^{-A_{00}} - \frac{2}{A_{00}^4}+\frac{1}{A_{00}^3}\right]\right. \\ &\quad \left. + CA_{01}\left[\left(\frac{1}{A_{00}^4}+\frac{1}{A_{00}^3}\right)\mathrm{e}^{-A_{00}} - \frac{1}{A_{00}^4}\right]\right\} + O(\epsilon^2), \end{aligned} \tag{5.4}$$

and the dimensionless momentum drag is

$$\begin{aligned} F_m^* &= \frac{2\pi}{\epsilon}\int_0^\pi (u_{g,r}^2\cos\theta - u_{g,r}u_{g,\theta}\sin\theta)\big|_{r=1}\sin\theta\,\mathrm{d}\theta \\ &= -\frac{4\pi}{3}\left\{3A_{00}+A_{00}A_{11}+C\left[\left(\frac{1}{A_{00}^3}+\frac{1}{A_{00}^2}\right)\mathrm{e}^{-A_{00}} - \frac{1}{A_{00}^3}+\frac{1}{2A_{00}}\right]\right\} \\ &\quad - \frac{4\pi}{3}\epsilon\left\{3A_{01}+A_{00}A_{12}+A_{01}A_{11}+2C_1\left[\left(\frac{1}{A_{00}^3}+\frac{1}{A_{00}^2}\right)\mathrm{e}^{-A_{00}} - \frac{1}{A_{00}^3}+\frac{1}{2A_{00}}\right]\right. \\ &\quad \left. + CA_{01}\left[\left(\frac{1}{A_{00}^4}+\frac{1}{A_{00}^3}-\frac{1}{A_{00}^2}\right)\mathrm{e}^{-A_{00}} - \frac{1}{A_{00}^4}+\frac{3}{2A_{00}^2}-\frac{1}{8A_{01}}\right]\right\} + O(\epsilon^2). \end{aligned} \tag{5.5}$$

The total drag is

$$\begin{aligned} F_T^* &= F_\mu^* + F_p^* + F_m^* \\ &= -\frac{4\pi}{3}\left\{3A_{00}+\frac{C}{2A_{00}}+\epsilon\left(3A_{01}+\frac{C_1}{A_{00}}+\frac{3CA_{01}}{2A_{00}^2}-\frac{C}{8}\right)\right\} + O(\epsilon^2). \end{aligned} \tag{5.6}$$

6. Solution for the temperature field: gaseous phase

The temperature is non-dimensionalized as $T_g^* = T_g c_{pg}/\Delta H_c$. Defining

$$g = \frac{T_g^* - T_\infty^*}{T_o^* - T_\infty^*} \quad \text{and} \quad h = Y_F \tag{6.1}$$

we get

$$Sc\left(A_{00}\boldsymbol{u}_{g0}+\epsilon\boldsymbol{u}_{g1}+\epsilon^2\boldsymbol{u}_{g2}\right)\cdot\nabla g-\nabla^2 g=0, \tag{6.2}$$

$$Sc\left(A_{00}\boldsymbol{u}_{g0}+\epsilon\boldsymbol{u}_{g1}+\epsilon^2\boldsymbol{u}_{g2}\right)\cdot\nabla h-\nabla^2 h=0. \tag{6.3}$$

In the outer region we have

$$g^o(\rho,\bar{\mu})=\sum_{n=0}^{\infty}F^n(\epsilon)G_n(\rho,\bar{\mu}). \tag{6.4}$$

6.1. *Leading-order outer solution*

Taking $F^0(\epsilon)=\epsilon$ the governing equation for G_0 becomes

$$\nabla_\rho^2 G_0-\bar{\mu}\frac{\partial G_0}{\partial\rho}-\frac{(1-\bar{\mu}^2)}{\rho}\frac{\partial G_0}{\partial\bar{\mu}}=0. \tag{6.5}$$

The solution can be obtained as (Gogos *et al.* 1986)

$$G_0=-\frac{\hat{\alpha}}{\rho Sc}\exp\left[-\tfrac{1}{2}Sc\rho(1-\bar{\mu})\right] \tag{6.6}$$

where $\hat{\alpha}=g_{s00}Sc\tilde{A}_{00}/(\mathrm{e}^{-\tilde{A}_{00}}-1)$ and $\tilde{A}_{00}=A_{00}Sc$.

6.2. *Leading-order inner solution*

A sufficiently general form is assumed for the inner expansion as

$$g^i(r,\bar{\mu})=\sum_{n=0}^{\infty}\sum_{m=0}^{\infty}f_n(\epsilon)g_{mn}(r)P_m(\bar{\mu}). \tag{6.7}$$

Taking $f_0(\epsilon)=1$ the governing equation becomes

$$\frac{\mathrm{d}^2 g_{m0}}{\mathrm{d}r^2}+\left(\frac{2}{r}-\frac{\tilde{A}_{00}}{r^2}\right)\frac{\mathrm{d}g_{m0}}{\mathrm{d}r}-\frac{m(m+1)}{r^2}g_{m0}=0. \tag{6.8}$$

The solution which matches with the outer solution is

$$g_{00}=g_{s00}\frac{\mathrm{e}^{-\tilde{A}_{00}/r}-1}{\mathrm{e}^{-\tilde{A}_{00}}-1}. \tag{6.9}$$

6.3. *First-order inner solution*

With $f_1(\epsilon)=\epsilon$ the solution for g_{m1} is

$$g_{01}=-\frac{\hat{\alpha}A_{01}}{\tilde{A}_{00}^{\,2}}\left(1+\frac{\tilde{A}_{00}}{r}\right)\mathrm{e}^{-\tilde{A}_{00}/r}+B_{11}\mathrm{e}^{-\tilde{A}_{00}/r}+B_{12}, \tag{6.10}$$

$$g_{11}=[B_{21}+\bar{V}(r)](r+\tfrac{1}{2}\tilde{A}_{00})\mathrm{e}^{-\tilde{A}_{00}/r}+[B_{22}+\bar{U}(r)](r-\tfrac{1}{2}\tilde{A}_{00}), \tag{6.11}$$

where

$$\bar{U}(r)=\frac{4\hat{\alpha}}{\tilde{A}_{00}^{\,3}}\int_1^r(r+\tfrac{1}{2}\tilde{A}_{00})\frac{f(r)}{r^2}\mathrm{e}^{-\tilde{A}_{00}/r}\mathrm{d}r,$$

$$\bar{V}(r)=-\frac{4\hat{\alpha}}{\tilde{A}_{00}^{\,3}}\int_1^r(r-\tfrac{1}{2}\tilde{A}_{00})\frac{f(r)}{r^2}\mathrm{d}r.$$

The expressions for Ω, B_{11}, B_{12}, B_{21}, and B_{22} can be found in Gogos *et al.* (1986).

6.4. *First-order outer solution*

The governing equation for G_1 is obtained as

$$\nabla_\eta^2 G_1 - \bar{\mu}\frac{\partial G_1}{\partial \eta} - \frac{(1-\bar{\mu}^2)}{\eta}\frac{\partial G_1}{\partial \bar{\mu}}$$
$$= \frac{Sc\hat{\alpha}C}{12A_{00}}\frac{1}{\eta^3}\left[(1+Sc)+\frac{2Sc}{\eta}+(1-Sc)\bar{\mu}\right]\exp\left[-\frac{1}{2}\eta\left(\frac{(Sc+1)}{Sc}\right)(1-\bar{\mu})\right]$$
$$+ Sc^2\hat{\alpha}\left(A_{00}-\frac{C}{6A_{00}}\right)\frac{1}{\eta^3}\left(\frac{1}{2}+\frac{1}{\eta}-\frac{\bar{\mu}}{2}\right)\exp[-\tfrac{1}{2}\eta(1-\bar{\mu})] \tag{6.12}$$

where $\eta = \rho Sc$. Now letting $G_1(\eta,\bar{\mu}) = \exp(\frac{1}{2}\eta\bar{\mu})G_1^*(\eta,\bar{\mu})$ we get

$$(\nabla_\eta^2 - \tfrac{1}{4})G_1^* = \frac{Sc^2\hat{\alpha}C}{12A_{00}}\frac{1}{\eta^3}\left[\frac{(1+Sc)}{Sc}+\frac{2}{\eta}+\frac{(1-Sc)}{Sc}\bar{\mu}\right]\exp\left[-\frac{1}{2}\eta\left(\frac{(Sc+1-\bar{\mu})}{Sc}\right)\right]$$
$$-\frac{Sc^2\hat{\alpha}C}{12A_{00}}\frac{1}{\eta^3}\left(1+\frac{2}{\eta}-\bar{\mu}\right)\exp[-\tfrac{1}{2}\eta]+\frac{Sc^2\hat{\alpha}A_{00}}{2}\frac{1}{\eta^3}\left(1+\frac{2}{\eta}-\bar{\mu}\right)\exp[-\tfrac{1}{2}\eta]. \tag{6.13}$$

G_1^* is expanded in terms of Legendre polynomials as

$$G_1^*(\eta,\bar{\mu}) = \sum_{n=0}^{\infty} F_n(\eta)P_n(\bar{\mu}). \tag{6.14}$$

Using

$$e^{\eta\bar{\mu}/(2Sc)} = (2\pi)^{1/2}\sum_{n=0}^{\infty}(n+\tfrac{1}{2})\left(\frac{\eta}{2Sc}\right)^{-1/2} I_{n+1/2}\left(\frac{\eta}{2Sc}\right)P_n(\bar{\mu}), \tag{6.15}$$

$$\bar{\mu}e^{\eta\bar{\mu}/(2Sc)} = (2\pi)^{1/2}\sum_{n=0}^{\infty} n(n+\tfrac{1}{2})\left(\frac{\eta}{2Sc}\right)^{-3/2} I_{n+1/2}\left(\frac{\eta}{2Sc}\right)P_n(\bar{\mu})$$
$$+(2\pi)^{1/2}\sum_{n=0}^{\infty}(n+\tfrac{1}{2})\left(\frac{\eta}{2Sc}\right)^{-1/2} I_{n+3/2}\left(\frac{\eta}{2Sc}\right)P_n(\bar{\mu}), \tag{6.16}$$

the solution for equation (6.13) is obtained as

$$F_n = A_n'\eta^{-1/2}K_{n+1/2}(\tfrac{1}{2}\eta)+\frac{Sc\hat{\alpha}C}{9A_{00}}\eta^{-1/2}K_{n+1/2}(\tfrac{1}{2}\eta)\int_\eta^\infty I_{n+1/2}(\tfrac{1}{2}\eta)L_n(\eta)\mathrm{d}\eta$$
$$-\frac{Sc\hat{\alpha}C}{9A_{00}}\eta^{-1/2}I_{n+1/2}(\tfrac{1}{2}\eta)\int_\eta^\infty K_{n+1/2}(\tfrac{1}{2}\eta)L_n(\eta)\mathrm{d}\eta, \tag{6.17}$$

where

$$L_n(\eta) = \eta^{-5/2}e^{-\eta/2}\left[(1+\tfrac{1}{2}\eta)\,\delta_{n0}-\tfrac{1}{2}\eta\delta_{n1}\right]$$
$$+\tfrac{3}{2}(2n+1)\pi^{1/2}Sc^{3/2}\eta^{-3}e^{-\eta(Sc+1)/(2Sc)}$$
$$\times\left[\left(1+\eta\frac{Sc+1}{2Sc}-nSc+n\right)I_{n+1/2}\left(\frac{\eta}{2Sc}\right)-\eta\frac{Sc-1}{2Sc}I_{n+3/2}\left(\frac{\eta}{2Sc}\right)\right] \tag{6.18}$$

and $K_{n+1/2}(\eta/2)$, $I_{n+1/2}(\eta/2)$ are modified Bessel functions. The quantity δ_{ij} denotes the Kronecker delta function.

As $\rho \to 0$, $F_n(\rho Sc)$ behaves as

$$F_n \sim \hat{A}_n \rho^{-1/2} K_{n+1/2}(\tfrac{1}{2}\rho Sc) + \Gamma_n(\rho) + o(1) \tag{6.19}$$

where

$$\Gamma_0 = \frac{\hat{\alpha}A_{00}}{2\rho^2} + \left(\frac{\hat{\alpha}C\omega_0(Sc)}{9A_{00}} - \frac{\hat{\alpha}\tilde{A}_{00}}{4}\right)\frac{1}{\rho} - \frac{Sc\hat{\alpha}C}{18A_{00}}\ln\rho + \frac{\hat{\alpha}\tilde{A}_{00}Sc}{16} + \frac{Sc\hat{\alpha}C}{9A_{00}}\left(\frac{1}{2}\omega_0(Sc) + \frac{7}{6} - \frac{\gamma}{2}\right),$$

$$\Gamma_1 = -\frac{\hat{\alpha}A_{00}}{2\rho^2} + \left(\frac{\hat{\alpha}\tilde{A}_{00}}{4} - \frac{\hat{\alpha}C}{12A_{00}}\right)\frac{1}{\rho} - \frac{\hat{\alpha}\tilde{A}_{00}Sc}{16} + \frac{\hat{\alpha}C}{48A_{00}},$$

$$\Gamma_2 = \frac{\hat{\alpha}CSc}{216A_{00}} - \frac{\hat{\alpha}C}{144A_{00}},$$

$\omega_0(Sc) = -\frac{1}{4}Sc^2 + \frac{1}{8}Sc + \frac{1}{4}(Sc+1)^2(Sc-2)\ln[(Sc+1)/Sc] - \frac{1}{2}\ln Sc$.

In view of the large-r behaviour of expressions (6.9), (6.10), and (6.11) we choose

$$\hat{A}_0 = \left[\frac{\hat{\alpha}\tilde{A}_{00}}{4} - \omega_0(Sc) - B_{11}\tilde{A}_{00}\right]\left(\frac{Sc}{\pi}\right)^{1/2},\quad \hat{A}_1 = \frac{\hat{\alpha}\tilde{A}_{00}}{4}\left(\frac{Sc}{\pi}\right)^{1/2},\quad \hat{A}_n = 0 \text{ for } n \geqslant 2. \tag{6.20}$$

Hence, as $\rho \to 0$

$$G_1 \sim \left[\frac{\hat{\alpha}A_{00}}{2\rho^2} - \frac{B_{11}\tilde{A}_{00}}{\rho} - \frac{\hat{\alpha}ScC}{18A_{00}}\ln\rho + \frac{B_{11}\tilde{A}_{00}Sc}{2} + \frac{Sc\hat{\alpha}C}{9A_{00}}\left(\omega_0(Sc) + \frac{25}{24} - \frac{\gamma}{2}\right)\right]P_0(\bar{\mu}) + \left[\left(\frac{\hat{\alpha}\tilde{A}_{00}}{2} - \frac{\hat{\alpha}C}{12A_{00}}\right)\frac{1}{\rho} - \frac{Sc\tilde{A}_{00}B_{11}}{2} + \frac{\hat{\alpha}C}{48A_{00}} - \frac{\hat{\alpha}\tilde{A}_{00}Sc}{8}\right]P_1(\bar{\mu}) + \left[\frac{\hat{\alpha}Sc\tilde{A}_{00}}{8} - \frac{5\hat{\alpha}ScC}{216A_{00}} - \frac{\hat{\alpha}C}{144A_{00}} + \cdots\right]P_2(\bar{\mu}) + o(1). \tag{6.21}$$

6.5. *Second-order inner solution*

From the behaviour of the outer solution G_1 as $\rho \to 0$ which has terms like $\ln\rho$, it is clear that $f_2(\epsilon) = \epsilon^2 \ln\epsilon$. The governing equation to $O(\epsilon^2 \ln\epsilon)$ is

$$\left(\mathrm{D}_r^2 - \frac{\tilde{A}_{00}}{r^2}\frac{\partial}{\partial r}\right)g_{2*} = 0. \tag{6.22}$$

In view of equation (6.19) the solution is

$$g_{2*} = C_{21*} + C_{22*}\mathrm{e}^{-\tilde{A}_{00}/r}. \tag{6.23}$$

Taking $f_3(\epsilon) = \epsilon^2$ and expanding g_2^i in terms of Legendre polynomials as

$$g_2^i = \sum_{m=0}^{\infty} g_{m2}(r)P_m(\bar{\mu}), \tag{6.24}$$

we get for $m = 0$

$$\frac{\mathrm{d}^2 g_{02}}{\mathrm{d}r^2} + \left(\frac{2}{r} - \frac{\tilde{A}_{00}}{r^2}\right)\frac{\mathrm{d}g_{02}}{\mathrm{d}r} = R_0(r), \tag{6.25}$$

where R_0 is

$$R_0(r) = \frac{ScA_{02}}{r^2}\frac{\mathrm{d}g_{00}}{\mathrm{d}r} + \frac{Scf(r)}{3r^2}\frac{\mathrm{d}g_{11}}{\mathrm{d}r} + \frac{Scg_{11}}{3r^2}\frac{\mathrm{d}f(r)}{\mathrm{d}r} + \frac{ScA_{01}}{r^2}\frac{\mathrm{d}g_{01}}{\mathrm{d}r}. \tag{6.26}$$

The general solution is obtained as

$$g_{02} = C_{01}e^{-\tilde{A}_{00}/r} + C_{02} + \frac{e^{-\tilde{A}_{00}/r}}{\tilde{A}_{00}} \int_1^r r^2 e^{\tilde{A}_{00}/r} R_0(r)dr - \frac{1}{\tilde{A}_{00}} \int_1^r r^2 R_0(r)dr. \tag{6.27}$$

For $m = 1$ we have

$$\frac{d^2 g_{12}}{dr^2} + \left(\frac{2}{r} - \frac{\tilde{A}_{00}}{r^2}\right) \frac{dg_{12}}{dr} - \frac{2}{r^2} g_{12} = R_1(r), \tag{6.28}$$

where R_1 is

$$R_1(r) = \frac{Scf(r)}{r^2} \frac{dg_{01}}{dr} + \frac{2Sc\psi_{g2}^1(r)}{r^2} \frac{dg_{00}}{dr} + \frac{ScA_{01}}{r^2} \frac{dg_{11}}{dr}. \tag{6.29}$$

The solution is

$$\begin{aligned} g_{12} = {} & C_{11}(r + \tfrac{1}{2}\tilde{A}_{00})e^{-\tilde{A}_{00}/r} + C_{12}(r - \tfrac{1}{2}\tilde{A}_{00}) \\ & - \frac{4}{\tilde{A}_{00}^3}(r + \tfrac{1}{2}\tilde{A}_{00})e^{-\tilde{A}_{00}/r} \int_1^r (r - \tfrac{1}{2}\tilde{A}_{00}) r^2 R_1(r) e^{\tilde{A}_{00}/r} dr \\ & + \frac{4}{\tilde{A}_{00}^3}(r - \tfrac{1}{2}\tilde{A}_{00}) \int_1^r (r + \tfrac{1}{2}\tilde{A}_{00}) r^2 R_1(r) dr. \end{aligned} \tag{6.30}$$

g_{22} satisfies

$$\frac{d^2 g_{22}}{dr^2} + \left(\frac{2}{r} - \frac{\tilde{A}_{00}}{r^2}\right) \frac{dg_{22}}{dr} - \frac{6}{r^2} g_{22} = R_2(r), \tag{6.31}$$

where

$$R_2(r) = 2Sc \left[-\frac{f(r)}{3r^2} \frac{dg_{11}}{dr} - \frac{\psi_{g2}^2(r)}{r^2} \frac{dg_{00}}{dr} + \frac{g_{11}}{6r^2} \frac{df(r)}{dr} \right]. \tag{6.32}$$

The general solution for g_{22} is

$$\begin{aligned} g_{22} = {} & C_{21} \left(1 + \frac{6r}{\tilde{A}_{00}} + \frac{12r^2}{\tilde{A}_{00}^2}\right) e^{-\tilde{A}_{00}/r} + C_{22} \left(1 - \frac{6r}{\tilde{A}_{00}} + \frac{12r^2}{\tilde{A}_{00}^2}\right) \\ & + \left(1 + \frac{6r}{\tilde{A}_{00}} + \frac{12r^2}{\tilde{A}_{00}^2}\right) e^{-\tilde{A}_{00}/r} \int_1^r \frac{r^2}{\tilde{A}_{00}} \left(1 - \frac{6r}{\tilde{A}_{00}} + \frac{12r^2}{\tilde{A}_{00}^2}\right) R_2(r) e^{\tilde{A}_{00}/r} dr \\ & - \left(1 - \frac{6r}{\tilde{A}_{00}} + \frac{12r^2}{\tilde{A}_{00}^2}\right) \int_1^r \frac{r^2}{\tilde{A}_{00}} \left(1 + \frac{6r}{\tilde{A}_{00}} + \frac{12r^2}{\tilde{A}_{00}^2}\right) R_2(r) dr. \end{aligned} \tag{6.33}$$

After lengthy manipulations, the large-r behaviour is obtained as

$$g_{02} \sim -\frac{\hat{\alpha}Sc}{6} r - \frac{\hat{\alpha}ScC}{18A_{00}} \ln r + C_{01} + C_{02} + \Omega_0 + \cdots, \tag{6.34}$$

$$g_{12} \sim (C_{11} + C_{12} + \Omega_1) r - \frac{\tilde{A}_{00}}{2}(ScB_{11} + C_{11} + C_{12} + \Omega_1) + \frac{\hat{\alpha}C}{48A_{00}} + \cdots, \tag{6.35}$$

$$\begin{aligned} g_{22} \sim {} & \frac{12}{\tilde{A}_{00}^2}(C_{21} + C_{22} + \Omega_2) r^2 - \frac{6}{\tilde{A}_{00}}(C_{21} + C_{22} + \Omega_2) r + \frac{\hat{\alpha}Sc}{12} r \\ & + \frac{\hat{\alpha}Sc\tilde{A}_{00}}{8} - \frac{\hat{\alpha}C}{144A_{00}} - \frac{5\hat{\alpha}ScC}{216A_{00}} + (C_{21} + C_{22} + \Omega_2) + \cdots, \end{aligned} \tag{6.36}$$

where

$$\Omega_0 = \frac{\hat{\alpha}A_{02}}{\tilde{A}_{00}}\left[1 - \frac{1}{\tilde{A}_{00}} + \frac{e^{-\tilde{A}_{00}}}{\tilde{A}_{00}}\right] + \frac{ScA_{01}}{\tilde{A}_{00}}\left[-\frac{\hat{\alpha}A_{01}}{2}\left(1 + \frac{2e^{-\tilde{A}_{00}}}{\tilde{A}_{00}}\right) + B_{11}\left(\tilde{A}_{00} - 1 + e^{-\tilde{A}_{00}}\right)\right]$$
$$+ \lim_{r\to\infty}\left[\frac{\hat{\alpha}Sc}{6}r + \frac{\hat{\alpha}ScC}{18A_{00}}\ln r + \frac{Sce^{-\tilde{A}_{00}/r}}{3}\int_1^r \frac{g_{11}f(r)}{r^2}e^{\tilde{A}_{00}/r}dr\right], \tag{6.37}$$

$$\Omega_1 = \frac{2}{\tilde{A}_{00}^2}\int_1^\infty \sum_{n=2}^{\infty}\left(-\frac{\tilde{A}_{00}}{r}\right)^n \frac{(n-1)}{(n+1)!}R_1(r)r^2e^{\tilde{A}_{00}/r}dr, \tag{6.38}$$

$$\Omega_2 = -\frac{1}{\tilde{A}_{00}}\int_1^\infty \sum_{n=3}^{\infty}\left(-\frac{\tilde{A}_{00}}{r}\right)^n \frac{(n-1)(n-2)}{(n+2)!}R_2(r)r^2e^{\tilde{A}_{00}/r}dr. \tag{6.39}$$

The matching condition is

$$\lim_{r\to\infty}\left[g_{00} + \epsilon\sum_{n=0}^{1} g_{n1}P_n(\bar{\mu}) + \epsilon^2\ln\epsilon g_{2*} + \epsilon^2\sum_{n=0}^{2} g_{n2}P_n(\bar{\mu})\right] \to \lim_{\rho\to 0}\left[\epsilon G_0 + \epsilon^2 G_1\right]. \tag{6.40}$$

Carrying out the matching up to and including $O(\epsilon^2)$ we get the following conditions:

$$C_{01} + C_{02} = \frac{B_{11}\tilde{A}_{00}Sc}{2} + \frac{Sc\hat{\alpha}C}{9A_{00}}\left(\omega_0(Sc) + \frac{25}{24} - \frac{\gamma}{2}\right) - \Omega_0, \tag{6.41}$$

$$C_{11} + C_{12} = \frac{\hat{\alpha}Sc}{4} - \Omega_1, \tag{6.42}$$

$$C_{21*} + C_{22*} = -\frac{\hat{\alpha}ScC}{18A_{00}}, \tag{6.43}$$

$$C_{21} + C_{22} = -\Omega_2. \tag{6.44}$$

These matching conditions can be used with the boundary conditions to calculate the constants of integration C_{ij}:

$$C_{01} = \frac{g_{s02}}{e^{-\tilde{A}_{00}} - 1} - \frac{1}{e^{-\tilde{A}_{00}} - 1}\left[\frac{B_{11}\tilde{A}_{00}Sc}{2} + \frac{Sc\hat{\alpha}C}{9A_{00}}\left(\omega_0(Sc) + \frac{25}{24} - \frac{\gamma}{2}\right) - \Omega_0\right], \tag{6.45}$$

$$C_{02} = -\frac{g_{s02}}{e^{-\tilde{A}_{00}} - 1} + \frac{e^{-\tilde{A}_{00}}}{e^{-\tilde{A}_{00}} - 1}\left[\frac{B_{11}\tilde{A}_{00}Sc}{2} + \frac{Sc\hat{\alpha}C}{9A_{00}}\left(\omega_0(Sc) + \frac{25}{24} - \frac{\gamma}{2}\right) - \Omega_0\right], \tag{6.46}$$

$$C_{11} = \frac{-g_{s12} + \left(\frac{1}{4}\hat{\alpha}Sc - \Omega_1\right)\left(1 - \frac{1}{2}\tilde{A}_{00}\right)}{1 - \frac{1}{2}\tilde{A}_{00} - e^{-\tilde{A}_{00}}\left(1 + \frac{1}{2}\tilde{A}_{00}\right)}, \tag{6.47}$$

$$C_{12} = \frac{g_{s12} - \left(\frac{1}{4}\hat{\alpha}Sc - \Omega_1\right)\left(1 + \frac{1}{2}\tilde{A}_{00}\right)e^{-\tilde{A}_{00}}}{1 - \frac{1}{2}\tilde{A}_{00} - e^{-\tilde{A}_{00}}\left(1 + \frac{1}{2}\tilde{A}_{00}\right)}, \tag{6.48}$$

$$C_{21*} = -\frac{\hat{\alpha}ScCe^{-\tilde{A}_{00}}}{18A_{00}\left(e^{-\tilde{A}_{00}} - 1\right)}, \tag{6.49}$$

$$C_{22*} = \frac{\hat{\alpha}ScC}{18A_{00}\left(e^{-\tilde{A}_{00}} - 1\right)}, \tag{6.50}$$

$$C_{21} = \frac{g_{s22} + \left(1 - \frac{6}{\tilde{A}_{00}} + \frac{12}{\tilde{A}_{00}^2}\right)\Omega_2}{\left(1 + \frac{6}{\tilde{A}_{00}} + \frac{12}{\tilde{A}_{00}^2}\right)e^{-\tilde{A}_{00}} - \left(1 - \frac{6}{\tilde{A}_{00}} + \frac{12}{\tilde{A}_{00}^2}\right)}, \tag{6.51}$$

$$C_{22} = -\frac{g_{s22} + \left(1 + \frac{6}{\tilde{A}_{00}} + \frac{12}{\tilde{A}_{00}^2}\right)\Omega_2 e^{-\tilde{A}_{00}}}{\left(1 + \frac{6}{\tilde{A}_{00}} + \frac{12}{\tilde{A}_{00}^2}\right)e^{-\tilde{A}_{00}} - \left(1 - \frac{6}{\tilde{A}_{00}} + \frac{12}{\tilde{A}_{00}^2}\right)}. \tag{6.52}$$

The expressions for the coupled variable h are identical to those for g and can be obtained by replacing the integration constants C_{ij} by constants d_{ij} in equations (6.27), (6.30), and (6.33).

The radial velocity at the droplet surface is related to the fuel mass fraction through the impermeability condition:

$$A_{00} = -\frac{1}{Sc}\ln[1 - h_{s00}], \tag{6.53}$$

$$A_{01} = \frac{h_{s01}}{Sc((1/\nu_F) + Y_{O\infty} - h_{s00})} - \frac{1}{2}\ln[1 - h_{s00}], \tag{6.54}$$

$$A_{11} = \frac{1}{1 - \frac{1}{2}\tilde{A}_{00} - e^{-\tilde{A}_{00}}\left(1 + \frac{1}{2}\tilde{A}_{00}\right)} \times \left[\frac{\tilde{A}_{00}^3}{4}(1 + \Omega) + \frac{A_{00}(1 - \frac{1}{2}\tilde{A}_{00}) + (e^{-\tilde{A}_{00}} - 1)}{1 - h_{s00}}h_{s11}\right] \tag{6.55}$$

$$A_{02} = \frac{\tilde{A}_{00}h_{s02} + \frac{1}{3}\tilde{A}_{11}h_{s11} - d_{01}\tilde{A}_{00}e^{-\tilde{A}_{00}}}{Sc(1 - h_{s00})}, \tag{6.56}$$

$$A_{12} = \frac{\tilde{A}_{00}h_{s12} + \tilde{A}_{11}h_{s01} + \tilde{A}_{01}h_{s11}}{Sc(1 - h_{s00})} - \frac{d_{11}(1 + \tilde{A}_{00} + \frac{1}{2}\tilde{A}_{00}^2)e^{-\tilde{A}_{00}} + d_{12}}{Sc(1 - h_{s00})}, \tag{6.57}$$

$$A_{22} = \frac{\tilde{A}_{00}h_{s22} + \frac{2}{3}\tilde{A}_{11}h_{s11}}{Sc(1 - h_{s00})} + \frac{-d_{21}\left(\tilde{A}_{00}^3 + 6\tilde{A}_{00}^2 + 18\tilde{A}_{00} + 24\right)e^{-\tilde{A}_{00}} + d_{22}\left(-6\tilde{A}_{00} + 24\right)}{\tilde{A}_{00}^2 Sc(1 - h_{s00})}, \tag{6.58}$$

where $\tilde{A}_{11} = ScA_{11}$. The integration constants d_{ij} are obtained by replacing g_{sij} with h_{sij} in the expressions for C_{ij}.

The fuel mass fraction and the temperature at the drop surface can be expanded as

$$Y_{F,s} = h_{s00} + \epsilon(h_{s01} + \bar{\mu}h_{s11}) + \epsilon^2(h_{s02} + \bar{\mu}h_{s12} + \tfrac{1}{2}(3\bar{\mu}^2 - 1)h_{s22}) + \cdots, \tag{6.59}$$

$$T_s = T_{s00} + \epsilon(T_{s01} + \bar{\mu}T_{s11}) + \epsilon^2(T_{s02} + \bar{\mu}T_{s12} + \tfrac{1}{2}(3\bar{\mu}^2 - 1)T_{s22}) + \cdots. \tag{6.60}$$

Substituting these expressions into the Clausius–Clapeyron equation and expanding in ϵ, with T_b denoting the boiling temperature, we get

$$h_{s00} = \frac{\exp\left[\chi\left(\frac{1}{T_b} - \frac{1}{T_{s00}}\right)\right]}{r_w - (r_w - 1)\exp\left[\chi\left(\frac{1}{T_b} - \frac{1}{T_{s00}}\right)\right]}, \tag{6.61}$$

$$h_{s01} = h_{s00}\frac{T_{s01}}{T_{s00}^2}\chi(1-\xi), \tag{6.62}$$

$$h_{s11} = h_{s00}\frac{T_{s11}}{T_{s00}^2}\chi(1-\xi), \tag{6.63}$$

$$h_{s02} = h_{s00}\frac{\chi(1-\xi)}{T_{s00}^2}\left[T_{s02} - \frac{T_{s01}^2}{T_{s00}} - \frac{T_{s11}^2}{3T_{s00}}\right] + h_{s00}\frac{\chi^2(1-\xi+2\xi^2)}{2T_{s00}^4}\left[T_{s01}^2 + \frac{T_{s11}^2}{3}\right], \tag{6.64}$$

$$h_{s12} = h_{s00}\frac{\chi(1-\xi)}{T_{s00}^2}\left[T_{s12} - \frac{2T_{s01}T_{s11}}{T_{s00}} + \chi\frac{(1-\xi+2\xi^2)}{(1-\xi)}\frac{T_{s01}T_{s11}}{T_{s00}^2}\right], \tag{6.65}$$

$$h_{s22} = h_{s00}\frac{\chi(1-\xi)}{T_{s00}^2}\left[T_{s22} - \frac{2T_{s11}^2}{3T_{s00}} + \chi\frac{(1-\xi+2\xi^2)}{(1-\xi)}\frac{T_{s11}^2}{3T_{s00}^2}\right], \tag{6.66}$$

where

$$\xi = (1-r_w)\,Y_{F,s00}\,, \quad \chi = \frac{LW_F c_{pg}}{\bar{R}\Delta H_c}\,,$$

and

$$Y_{F,s00} = \frac{\exp\left[\chi\left(\frac{1}{T_b} - \frac{1}{T_{s00}}\right)\right]}{r_w - (r_w - 1)\exp\left[\chi\left(\frac{1}{T_b} - \frac{1}{T_{s00}}\right)\right]}\,.$$

7. Solution for the temperature field: liquid phase

The temperature inside the droplet is non-dimensionalized as $T_\ell^* = T_\ell c_{pg}/\Delta H_c$ and time is normalized as $t^* = \alpha_\ell t/R_0^2$. The governing equations are written in terms of the transformed variable g_ℓ:

$$g_\ell = \frac{T_\ell^* - T_\infty^*}{T_o^* - T_\infty^*}. \tag{7.1}$$

Similar to the expansion for the temperature in the gaseous phase, a perturbation scheme in terms of ϵ and Legendre polynomials is used:

$$g_\ell = g_{\ell 00} + \epsilon\,(g_{\ell 01} + P_1(\bar{\mu})g_{\ell 11}) + \epsilon^2\,(g_{\ell 02} + P_1(\bar{\mu})g_{\ell 12} + P_2(\bar{\mu})g_{\ell 22}) + \cdots. \tag{7.2}$$

This expansion along with equations (4.4) and (4.8) are substituted into equation (2.5). The resulting differential equations are solved numerically using a finite difference method. An implicit algorithm is used to solve for the transient temperature field inside the droplet. Calculations for the drop exterior are carried out simultaneously. At each time step, several iterations are required to obtain consistent convergent solutions.

8. Physical quantities

The mass burning rate at the droplet surface is given by

$$\dot{m} = 2\pi R\mu_g \int_{-1}^{1} u_r|_{r=1}\,\mathrm{d}\bar{\mu}\,. \tag{8.1}$$

Non-dimensionalizing the mass burning rate by $4\pi R\mu_g A_{00}$ gives

$$\dot{m} = 1 + \epsilon\frac{A_{01}}{A_{00}} + \epsilon^2\frac{A_{02}}{A_{00}} + o(\epsilon^2). \tag{8.2}$$

The drop regression rate is given by

$$\frac{\mathrm{d}}{\mathrm{d}t}\left(\frac{D^2}{D_o^2}\right) = -\frac{8k_g\tilde{A}_{00}}{(\rho_\ell - \rho_g)c_{pg}D_o^2}\left(1 + \epsilon\frac{A_{01}}{A_{00}} + \epsilon^2\frac{A_{02}}{A_{00}} + o(\epsilon^2)\right). \tag{8.3}$$

The heat quantities are non-dimensionalized by $4\pi R_0 k_g \Delta H_c/c_{pg}$. The dimensionless heat transfer from the gaseous phase to the droplet is

$$\begin{aligned} q_g &= -\frac{R}{2R_0}\int_{-1}^{1}\left.\frac{\partial T_g}{\partial r}\right|_{r=1}\mathrm{d}\bar{\mu} \\ &= -\frac{(T_0 - T_\infty)\tilde{A}_{00}\mathrm{e}^{-\tilde{A}_{00}}}{(R_0/R)}\left[\frac{\hat{\alpha}}{Sc\tilde{A}_{00}} + \epsilon\left(B_{11} - \frac{\hat{\alpha}A_{01}}{\tilde{A}_{00}}\right) + \epsilon^2\ln\epsilon C_{22*} + \epsilon^2 C_{01} + o(\epsilon^2)\right]. \end{aligned} \tag{8.4}$$

The heat required for fuel evaporation is

$$\begin{aligned} q_e &= -\frac{1}{2}\frac{R}{R_0}\frac{Sc}{\Delta H_c}\int_{-1}^{1} Lu_r|_{r=1}\,\mathrm{d}\bar{\mu} \\ &= -\frac{Sc}{Ja}\frac{R}{R_0}\left(A_{00} + \epsilon A_{01} + \epsilon^2 A_{02} + o(\epsilon^2)\right). \end{aligned} \tag{8.5}$$

In the above, $Ja = \Delta H_c/L$. The heat used for liquid heating is

$$q_\ell = q_g - q_e. \tag{8.6}$$

An equation for the velocity of the droplet can be obtained by setting the net force acting on the droplet (weight, drag, and buoyancy) equal to $m\,\mathrm{d}U_\infty/\mathrm{d}t$:

$$\begin{aligned} \frac{\mathrm{d}U_\infty}{\mathrm{d}t} = \phi_\mu Pr_\ell\left[3A_{00} + \frac{C}{2A_{00}} + \epsilon\left(3A_{01} + \frac{C_1}{A_{00}} + \frac{3CA_{01}}{2A_{00}^2} - \frac{C}{8}\right)\right]U_\infty \\ + \frac{gPr_\ell R_0}{v_g^2}R^2\left(\phi_v - \phi_\mu\right). \end{aligned} \tag{8.7}$$

9. Formulation: burning droplet

For the droplet burning situation, the governing equations are

$$\frac{\partial T_\ell}{\partial t} + \boldsymbol{u}_\ell \cdot \nabla T_\ell = \alpha_\ell \nabla^2 T_\ell, \tag{9.1}$$

$$\rho_g c_{pg}\boldsymbol{u}_g \cdot \nabla T_g - k_g\nabla^2 T_g = \Delta H_c\omega, \tag{9.2}$$

$$\rho_g \boldsymbol{u}_g \cdot \nabla Y_O - \rho_g D_g \nabla^2 Y_O = -W_O \nu_O \omega, \tag{9.3}$$

$$\rho_g \boldsymbol{u}_g \cdot \nabla Y_F - \rho_g D_g \nabla^2 Y_F = -W_F \nu_F \omega, \tag{9.4}$$

where ω is the reaction rate for the reaction

$$\nu_F F + \nu_O O \rightarrow \text{Products}. \tag{9.5}$$

The temperature and the mass fractions are non-dimensionalized as follows:

$T_g^* = T_g c_{pg}/\Delta H_c$, $Y_O^* = W_F Y_O/(v_O W_O)$ and $Y_F^* = Y_F/v_F$. Using equations (9.2), (9.3), and (9.4) and defining Shvab–Zeldovich variables as

$$g = \frac{T_g^* - T_\infty^* + Y_O^* - Y_{O\infty}^*}{T_o^* - T_\infty^* - Y_{O\infty}^*} \quad \text{and} \quad h = Y_F^* - Y_O^* + Y_{O\infty}^* \tag{9.6}$$

the governing equations for the coupled variables g and h become identical to the governing equations for the evaporation problem (equations (6.2) and (6.3)) for unity Lewis number in the continuous phase. Thus the mathematical procedures developed earlier can be used to obtain solutions for the temperature field and species distribution for a translating burning droplet. (For details, see Jog 1993.)

The non-dimensional variable g_ℓ for the temperature field inside the droplet is modified as

$$g_\ell = \frac{T_\ell^* - T_\infty^* - Y_{O\infty}}{T_o^* - T_\infty^* - Y_{O\infty}}. \tag{9.7}$$

10. Results and discussion

In this study, the combustion of a slowly moving liquid fuel droplet has been examined. The previous analyses (Gogos *et al.* 1986 and Sadhal & Ayyaswamy 1983) have been extended to include the effects of higher-order perturbations in the flow field as well as temperature and species transport. Inclusion of higher-order effects increases the mathematical complexities significantly as the evaluation of the flow field itself becomes a singular perturbation problem. Results are presented for quasi-steady combustion of a slowly moving droplet, and to make fruitful comparisons with the lower-order theory, calculations are made for *n*-heptane fuel in air as in Gogos *et al.* (1986). Detailed time histories of the burning drop and the drop hydrodynamics have been developed. The following property values are used in this study: $c_{pg} = 3.64$ kJ kg^{-1} K, $\rho_g = 0.6$ kg m^{-3}, $v_g = 0.4 \times 10^{-4}$ m^2 s^{-1}, $k_g = 5.73 \times 10^{-2}$ W m^{-1} K, $Pr = 1$, $Sc = 1$, $\rho_\ell = 650$ kg m^{-3}, $\alpha_\ell = 0.72 \times 10^{-7}$ m^2 s^{-1}, $\phi_\mu = 0.1$, $\phi_k = k_g/k_\ell = 0.84$, $L = 317$ kJ kg^{-1}, $T_b = 371.6$ K, $T_\infty = 298$ K, $Y_{O\infty} = 0.23$, $W_F = 100.2$, $r_w = 0.3$, $R_0 = 5.0 \times 10^{-4} m$, $v_F = 1$, $v_O = 11$, $\Delta H_c = 45{,}000$ kJ kg^{-1}.

Figure 2 shows the streamlines in the flow around the burning droplet for initial translational Reynolds number $\epsilon_0 = 0.2$ at non-dimensional time $t^* = \alpha_\ell t/R_0^2 = 0.1$. Results obtained by first-order theory are shown in the left half of the figure and the results of the higher-order theory are shown in the right half. Owing to the evaporation of fuel at the surface, streamlines originate at the droplet surface and follow the external flow. Near the front of the drop, the outward radial flow and the uniform external flow oppose each other forming a stagnation point as shown. For the parameters considered, the stagnation point is situated between the flame and the droplet surface. In the figure, streamlines *a*, *b*, *c*, *d* and *a'*, *b'*, *c'*, *d'* are drawn for identical locations on the drop surface, *e* and *e'* denote the streamlines that originate from the stagnation point. The stream functions for g and g' are identical in value. The primes denote results from second-order theory. The stream function values are shown in the figure caption. By comparing the values for *a*, *b*, *c*, *d* and *a'*, *b'*, *c'*, *d'*, it is seen that a larger mass efflux or higher rate of vaporization is predicted by the second-order theory. For identical conditions, the results of the higher-order theory predict the location of the flame front and of the forward stagnation point to be about 15 % closer to the drop surface than those predicted by the first-order theory. The flame is noted to be asymmetric but with varying degree of asymmetry. The asymmetry itself is a direct consequence of convection. The streamline *e* is farther

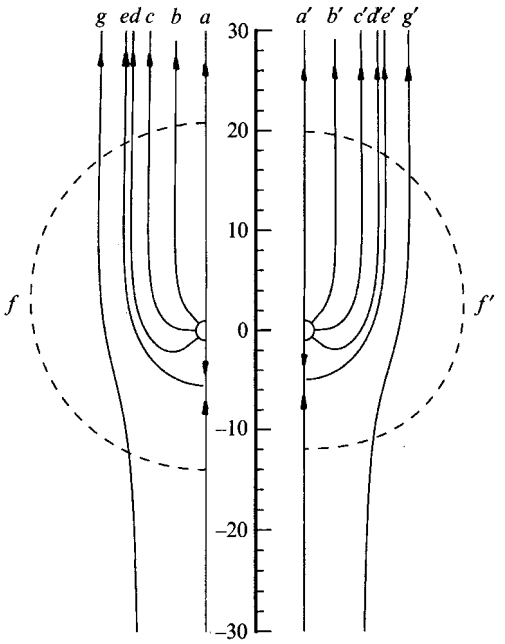

FIGURE 2. Calculated flow streamlines at non-dimensional time $t^* = 0.1$. $\epsilon_0 = 0.2$, $T_0 = 320$ K. The vertical scale graduations show multiples of the droplet radius. Solid lines: streamlines, dashed lines: flame front. Left half: first-order theory, right half: second-order theory. Stream function values: $a = -2.2600$, $b = -1.6074$, $c = -0.0150$, $d = 1.5050$, $e = 2.2600$, $g = 6.0$, f - flame, and $a' = -2.4800$, $b' = -1.7800$, $c' = -0.0498$, $d' = 1.6300$, $e' = 2.4800$, $g' = 6.0$, f' - flame.

removed from the drop centre than e', although the stream function values are the same for these lines. These observations are explained as follows. The second-order theory predicts a relatively smaller total drag (see figure 5) and a relatively higher rate of vaporization (see figure 7) compared to the first-order theory. With a smaller drag, the instantaneous translational velocity is higher. Higher vaporization rate, on the other hand, is accompanied by a stronger radial field. Also, the translational Reynolds number is decreasing because of the change in the size of the drop. These are all competing mechanisms in the determination of the locations of the forward stagnation point and of the flame. For the parameters under consideration, the increased translational velocity has caused the forward stagnation point to be closer to the drop surface and an increased degree of asymmetry for the flame.

The streamlines inside the droplet for two different non-dimensional times $t^* = 0.01$ and $t^* = 0.1$ are shown in figures 3(a) and 3(b), respectively. In each figure, the left half is the result of the first-order theory and the right half corresponds to the second order, and the streamlines shown are for identical stream function values calculated from each theory. The shear force at the droplet surface introduces circulatory motion in the liquid phase. The lower-order theory predicts an internal spherical vortex symmetrical about the horizontal axis for all times. On the other hand, the higher-order theory reveals asymmetry in the internal circulation. At $t^* = 0.01$, the deviation from symmetry is small. At a later time, $t^* = 0.1$, the internal vortex shifts more towards the front of the droplet with increased asymmetry. This behaviour is revealed by the inclusion of higher-order terms and can be explained as follows. The velocity field inside the droplet can be calculated from equations (4.4)

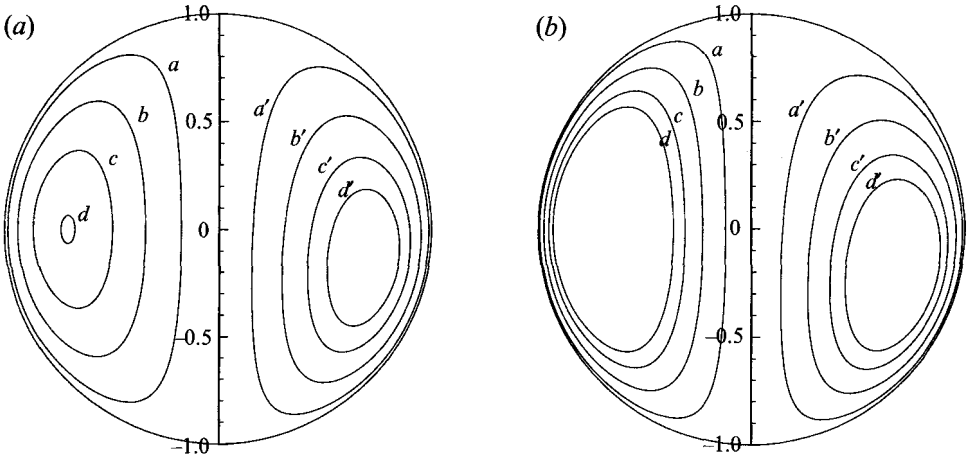

FIGURE 3. Streamlines inside the droplet at (a) $t^* = 0.01$ and (b) $t^* = 0.1$. $\epsilon_0 = 0.2$, $T_0 = 320K$. Left half: lower-order theory, right half: higher-order theory. Stream function values: $a = a' = 0.2155 \times 10^{-3}$, $b = b' = 0.7437 \times 10^{-3}$, $c = c' = 1.3090 \times 10^{-3}$, $d = d' = 1.7264 \times 10^{-3}$.

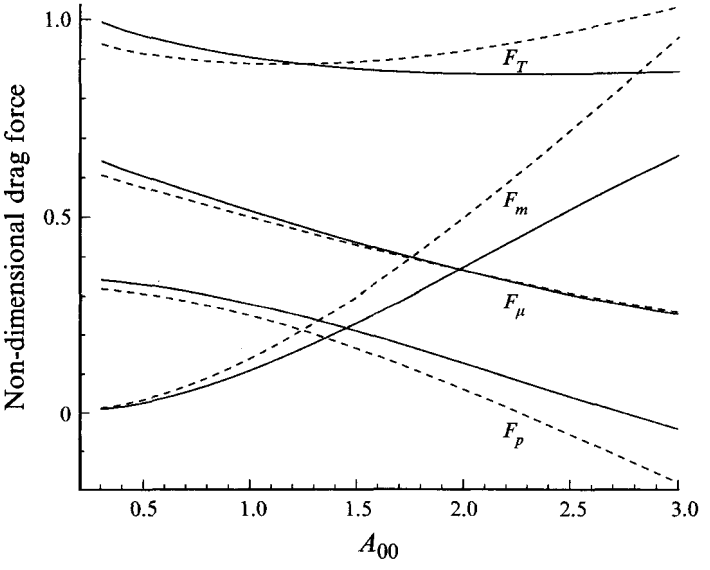

FIGURE 4. Variation of non-dimensional drag force with A_{00}. $\epsilon_0 = 0.2$. Solid lines: solutions up to $O(\epsilon^2)$, dashed lines: solutions up to $O(\epsilon)$.

and (4.8) as

$$u_{\ell,r} = 2\epsilon(\hat{B} + \epsilon B_1)(r^2 - 1)\bar{\mu} + \epsilon^2 B_2(r^3 - r)(3\bar{\mu}^2 - 1),$$
$$u_{\ell,\theta} = -\epsilon(\hat{B} + \epsilon B_1)(4r^2 - 2)(1 - \bar{\mu}^2)^{1/2} - \epsilon^2 B_2(5r^3 - 3r)\bar{\mu}(1 - \bar{\mu}^2)^{1/2}.$$

Clearly, the first terms in the above equations give rise to a velocity field symmetric about the equatorial plane corresponding to the Hill's spherical vortex. The second terms in the above equations introduce asymmetry in the velocity field. The value of the constant B_2 increases as the non-uniformity of the radial evaporation increases with time and this causes the shift of the internal vortex. As the radial evaporation

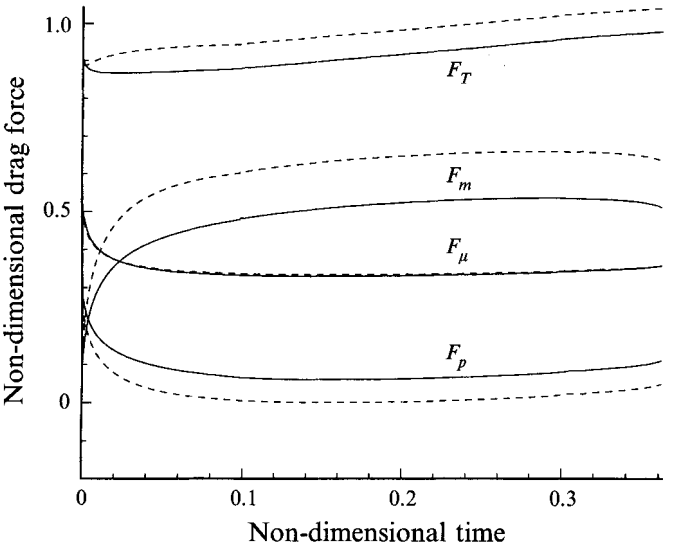

FIGURE 5. Variation of non-dimensional drag force with time. $\epsilon_0 = 0.2$ and $T_0 = 320$ K. Solid lines: solutions up to $O(\epsilon^2)$, dashed lines: solutions up to $O(\epsilon)$.

velocity increases, the strength of this circulatory vortex decreases. This is due to the convection of vorticity away from the drop surface.

Figure 4 shows the variation of each component of the drag force with radial Reynolds number, A_{00}. The solid lines show the results of the higher-order theory and the dashed lines correspond to first order. As the droplet moves and burns in the atmosphere, its temperature and the normal component of the velocity at the surface A_0, both increase. With increasing A_{00}, the total drag force decreases until a minimum is reached, and increases thereafter. The normal component of the interfacial velocity ($u_{g,r}|_{r=R}$) is maximum at the front and decreases towards the rear. The recoil effect of the flux leaving the droplet produces momentum drag. With increasing vaporization rate, the contribution of the momentum drag term becomes increasingly important. With increased evaporation, the pressure drag decreases due to the reduction in pressure drop from the front towards the rear stagnation point. For large enough A_{00}, the pressure at the rear may in fact be higher than that at the front giving rise to a negative pressure drag. The viscous drag also decreases with increasing A_{00} because of the blowing effect. A combination of all of the above effects results first in a reduction and then in an increase in total drag with increasing A_{00}.

Figure 5 shows the temporal variation of the non-dimensional drag forces acting on the fuel droplet. The radial Reynolds number, A_{00}, increases with increasing t^*. For the range of t^* covered in figure 5, A_{00} would vary from 0.8 to about 2.3 (based on our numerical calculations). With increasing time, $u_{g,r}|_{r=R}$ also increases. There is pressure recovery at the rear of the drop and consequently the pressure drag decreases with increasing t^*. The viscous drag also decreases owing to the increased blowing effect. The momentum transfer from the drop surface to the far stream is increased owing to the increased vaporization causing the thrust drag to increase. The combined effect is an essentially monotonic increase in the total drag force with time. A comparison with the first-order theory shows that the lower-order theory overpredicts the drag force on the droplet.

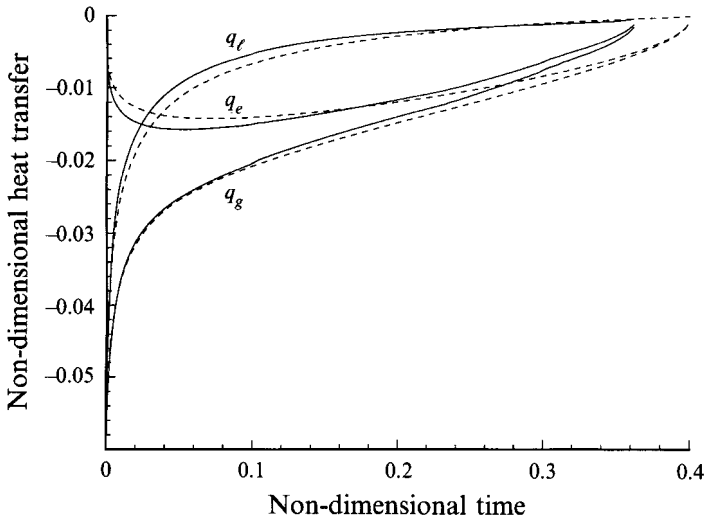

FIGURE 6. Variation of interfacial heat transport: q_g denotes heat transported towards the drop from the gaseous phase, q_ℓ denotes heat conducted into the interior of the drop, q_e denotes heat required for evaporation. $\epsilon_0 = 0.2$, $T_0 = 320$ K. Solid lines: solutions up to $O(\epsilon^2)$, dashed lines: solutions up to $O(\epsilon)$.

Figure 6 shows the temporal variation of the interfacial heat transport for a droplet introduced at $T_0 = 320$ K. The dashed lines show the results obtained from the first-order theory. Since the initial temperature of this droplet is less than the wet bulb temperature ($T_{wb} = 359.2$ K), a substantial portion of the energy received from the gaseous phase is used for liquid heating for about a third of the droplet lifetime. The dimensionless droplet lifetime predicted from higher-order theory is $t^* \approx 0.36$ and is $t^* \approx 0.4$ from first-order theory. It may be noted that the total droplet lifetime may be inferred from the figure as corresponding to the dimensionless time when the heat fluxes are zero. As the temperature of the droplet increases, the heat transport from the gaseous phase decreases whereas the evaporation velocity and the heat required for evaporation both increase. As expected, the results are qualitatively similar to those obtained from the first-order analysis. However, for identical conditions, the first-order analysis predicts the droplet lifetime to be about 12% longer than the higher-order analysis.

Recall that the variation of droplet diameter for combustion of a stationary fuel droplet is described by the well known d^2-law which predicts a linear variation of the square of the droplet diameter with time. Figure 7 shows the variation of the non-dimensional diameter squared with non-dimensional time for a droplet introduced at an initial temperature of 320 K, moving with an initial translatory Reynolds number of $\epsilon_0 = 0.2$, and at non-dimensional time $t^* = \alpha_\ell t/R_0^2$. During the initial transient period, the droplet heat-up leads to a lower rate of evaporation and this is evidenced by a lower slope of the d^2 curve. At later times, the droplet temperature increases and this results in a higher evaporation rate as shown by the increased slope. The second-order theory predicts a higher evaporation rate and a shorter droplet lifetime. By comparison with results for spherico-symmetric vaporization under identical conditions, translation is seen to shorten the droplet lifetime.

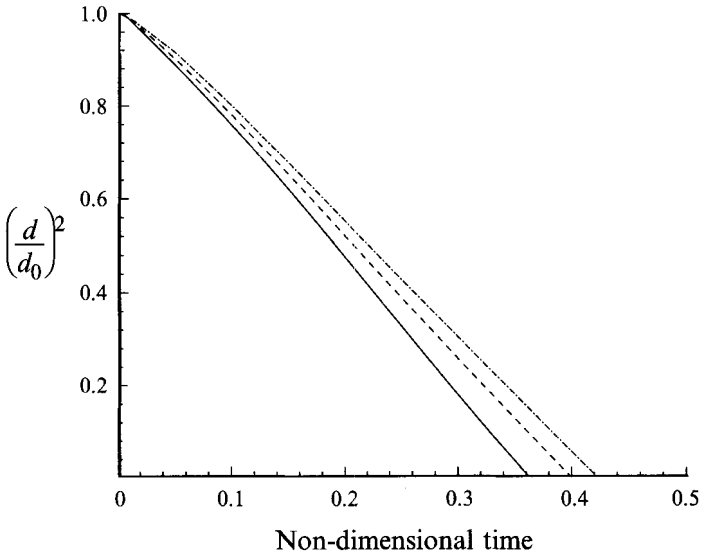

FIGURE 7. Variation of the square of the droplet diameter with time. $T_0 = 320$ K. Solid line: higher-order theory with $\epsilon_0 = 0.2$, dashed line: lower-order theory with $\epsilon_0 = 0.2$, and dashed-dotted line: $\epsilon = 0$, stationary droplet.

11. Conclusions

The evaporation/combustion of a slowly moving droplet has been analysed by coupled singular perturbation procedures. Results for the internal and external flow fields, drag coefficients, heat and species transport, and droplet lifetime have been developed correct to second order in the perturbation parameter. The chief motivation for the present study has been to develop elaborate mathematical details and results which can be directly incorporated in studies of ignition and extinction of a moving fuel droplet. Illustrative calculations have been provided for the vaporization and burning of an *n*-heptane droplet. Comparison of the results with those obtained by a first-order theory show that, for identical conditions, the higher-order theory predicts increased interfacial heat and mass transport and a smaller total drag force. Most significantly, the new theory shows that the flame stand-off distance is reduced, there is greater asymmetry in the flame structure, the forward stagnation point is closer, and the internal flow field is asymmetric. The droplet lifetime is predicted to be shorter. These features will have a significant impact on ignition/extinction studies since the location of the point of ignition/extinction will depend on them.

In a study of ignition, the temperature profiles obtained here for a vaporizing droplet will be valid in the entire flow field up to $O(\epsilon)$ as the nonlinear chemical reaction effects will be present only to $O(\epsilon^2)$. The temperature profiles in the reaction zone can therefore be perturbed by $O(\epsilon^2)$ from the frozen solutions. The governing equations for the perturbed temperature may then be solved, and ignition criteria may be obtained by appropriately matching the solutions with those obtained in this study correct to $O(\epsilon^2)$. A large change in the perturbed temperature for a small change in the Damköhler number would indicate the onset of ignition. By similar arguments, the results developed here for droplet combustion are useful for the determination of extinction characteristics. The structure of the flame zone can be studied by stretching the reaction zone around the flame front. The governing equations may be solved in

the reaction zone. Extinction criteria may be obtained by matching the temperature and the mass fraction variations in the reaction zone to the variations obtained in this paper for the inner and outer regions. The leakage of one of the reactants may be present in the higher-order solutions. In that circumstance, evaluation of the reactant leakage for different ambient conditions would predict droplet extinction.

It may be noted that the results presented here are of much wider applicability than for ignition/extinction studies. For example, diverse fields such as microgravity studies, atmospheric and aerosol sciences, and studies of material depletion from spherical particles would all benefit from the analysis presented here.

The authors are very grateful to Mr Srinivas Sripada, a doctoral student in the Department of Mechanical Engineering and Applied Mechanics at the University of Pennsylvania, for many helpful discussions.

REFERENCES

ABRAMZON, B. & SIRIGNANO, W. A. 1989 Droplet vaporization model for spray combustion calculations. *Intl J. Heat Mass Transfer* **32**, 1605–1618.

ACRIVOS, A. & TAYLOR, T. D. 1962 Heat and mass transfer from single sphere in Stokes flow. *Phys. Fluids* **5**, 387–394.

AGGARWAL, S. K., TONG, A. Y. & SIRIGNANO, W. A. 1984 A comparison of vaporization models in spray calculations. *AIAA J.* **22**, 1448–1457.

AVEDISIAN, C. T., YANG, J. C. & WANG, C. H. 1988 On low-gravity droplet combustion. *Proc. R. Soc. Lond.* A **420**, 183–200.

AYYASWAMY, P. S. 1995*a* Direct-contact transfer processes with moving liquid droplets. In *Advances in Heat Transfer* (ed. J. P. Hartnett *et al.*), vol. 26, pp. 1–104. Academic.

AYYASWAMY, P. S. 1995*b* Mathematical methods in direct-contact transfer studies with droplets. In *Annual Reviews of Heat Transfer* (ed. C. L. Tien), vol. 7. Begell House.

BUCKMASTER, J. D. 1985 *The Mathematics of Combustion.* SIAM.

BUCKMASTER, J. D. & LUDFORD, G. S. S. 1982 *Theory of Laminar Flames.* SIAM.

BUCKMASTER, J. D. & LUDFORD, G. S. S. 1983 *Lectures on Mathematical Combustion.* SIAM.

CHIGIER, N. A. 1983 Combustion models and laser diagnostic methods in sprays: A review. *Combust. Flame* **51**, 127–139.

CHUNG, J. N., AYYASWAMY, P. S. & SADHAL, S. S. 1984 Laminar condensation on a moving drop. Part 1. Singular perturbation technique. *J. Fluid Mech.* **139**, 105–130.

FAETH, G. M. 1983 Evaporation and combustion of sprays. *Prog. Energy Combust. Sci.* **9**, 1–76.

GOGOS, G. & AYYASWAMY, P. S. 1988 A model for the evaporation of a slowly moving droplet. *Combust. Flame* **74**, 111–129.

GOGOS, G., AYYASWAMY, P. S., SADHAL, S. S. & SUNDARARAJAN, T. 1986 Thin-flame theory for combustion of a moving liquid drop: effects due to variable density. *J. Fluid Mech.* **171**, 121–144.

HUBBARD, G. L., DENNY, V. E. & MILLS, A. F. 1975 Droplet evaporation: Effects of transients and variable properties. *Intl J. Heat Mass Transfer* **18**, 1003–1008.

JACKSON, G. S. & AVEDISIAN, C. T. 1994 The effect of initial diameter in spherically symmetric droplet combustion of sooting fuels. *Proc. R. Soc. Lond.* A **446**, 255–276.

JACKSON, G. S., AVEDISIAN, C. T. & YANG, J. C. 1991 Soot formation during combustion of unsupported methanol/toulene mixture droplets in microgravity. *Proc. R. Soc. Lond.* A **435**, 359–369.

JANSSEN, R. D. 1982 Drop combustion. PhD thesis, Cornell University.

JOG, M. A. 1993 Asymptotic and numerical studies of plasma arc heat transfer and phase change heat transfer. PhD thesis, University of Pennsylvania.

LAW, C. K. 1982 Recent advances in droplet vaporization and combustion. *Prog. Energy Combust. Sci.* **8**, 171–201.

LAW, C. K. & SIRIGNANO, W. A. 1977 Unsteady droplet combustion with droplet heating II: Conduction limit. *Combust. Flame* **28**, 175–186.

LIÑÁN, A. 1974 The asymptotic structure of counterflow diffusion flames for large activation energies. *Acta Astronautica* **1**, 1007–1039.

PRAKASH, S. & SIRIGNANO, W. A. 1980 Theory of convective droplet vaporization with unsteady heat transfer in the circulating phase. *Intl J. Heat Mass Transfer* **23**, 253–268.

PROUDMAN, I. & PEARSON, J. R. A. 1957 Expansion at small Reynolds number for the flow past a sphere and a circular cylinder. *J. Fluid Mech.* **2**, 237–262.

PRUPPACHER, H. R. & KLETT, J. D. 1980 *Microphysics of Clouds and Precipitation.* D. Reidel.

SADHAL, S. S. 1993 Solution to a class of transport problems with radially dominant convection. *Z. Angew Math. Phys.* **44**, 314–332.

SADHAL, S. S. & AYYASWAMY, P. S. 1983 Flow past a liquid drop with a large non-uniform velocity. *J. Fluid Mech.* **133**, 65–81.

SADHAL, S. S. & JOHNSON, R. E. 1986 On the deformation of drops and bubbles with varying interfacial tension. *Chem. Engng Commun.* **46**, 97–109.

SIRIGNANO, W. A. 1983 Fuel droplet vaporization and spray combustion theory. *Prog. Energy Combust. Sci.* **9**, 291–322.

SIRIGNANO, W. A. & LAW, C. K. 1978 Transient heating and liquid phase mass diffusion in fuel droplet vaporization. In *Evaporation Combustion of Fuels, Advances in Chemistry Series* (ed. J. T. Zhung), vol. 166, pp. 1–26. American Chemical Society.

SUNDARARAJAN, T. & AYYASWAMY, P. S. 1984 Heat and mass transfer associated with condensation on a moving drop: solutions for intermediate Reynolds numbers. *J. Fluid Mech.* **149**, 33–58.

WILLIAMS, A. 1973 Combustion of droplets of liquid fuels: a review. *Combust. Flame* **21**, 1–31.